EasyChair Preprint

№ 7957

Predicting the Energy and Exergy Performance of F135 PW100 Turbofan Engine via Deep Learning Approach

Mohammadreza Sabzehali, Amir Hossein Rabiee, Mahdi Alibeigia and Amir Mosavi

May 17, 2022

Predicting the energy and exergy performance of F135 PW100 turbofan engine via deep learning approach

Mohammadreza Sabzehali[a], Amir Hossein Rabiee*[b], Mahdi Alibeigi[a], Amir Mousavi[c]

[a] *Department of Mechanical Engineering, Tarbiat Modares University, PO Box 14115-143, Tehran, Iran*
[b] *School of Mechanical Engineering, Arak University of Technology, 38181-41167 Arak, Iran*
[c] *John von Neumann Faculty of Informatics, Obuda University, 1034 Budapest, Hungary*
**Corresponding Author's Email: rabiee@arakut.ac.ir*

Abstract

In the present study, the effects of flight-Mach number, flight altitude, fuel types, and intake air temperature on thrust specific fuel consumption, thrust, intake air mass flow rate, thermal and propulsive efficiecies, as well as the exergetic efficiency and the exergy destruction rate in F135 PW100 engine are investigated. Based on the results obtained in the first phase, to model the thermodynamic performance of the aforementioned engine cycle, Flight-Mach number and flight altitude are considered to be 2.5 and 30,000 m, respectively; due to the operational advantage of supersonic flying at high altitude flight conditions, and the higher thrust of hydrogen fuel. Accordingly, in the second phase, taking into account the mentioned flight conditions, an intelligent model has been obtained to predict output parameters (i.e., thrust, thrust specific fuel consumption, and overall exergetic efficiency) using the deep learning method. In the attained deep neural model, the pressure ratio of the high-pressure turbine, fan pressure ratio, turbine inlet temperature, intake air temperature, and bypass ratio are considered input parameters. The provided datasets are randomly divided into two sets: the first one contains 6079 samples for model training and the second set contains 1520 samples for testing. In particular, the Adam optimization algorithm, the cost function of the mean square error, and the active function of rectified linear unit are used to train the network. The results show that the error percentage of the deep neural model is equal to 5.02%, 1.43%, and 2.92% to predict thrust, thrust specific fuel consumption, and overall exergetic efficiency, respectively, which indicates the success of the attained model in estimating the output parameters of the present problem.

Keywords: Dual spool turbofan; F135 PW100; Mixed-flow turbofan; Deep learning; Energy and exergy.

Nomenclature

Cp	Specific heat capacity (J/kgK)	V_0	Flight speed (m/s)
Ex	Specific chemical Exergy of the fuel flow (kW)	W	Power output (kW)
ex	Airflow physical exergy (kJ/kg)	y_i	Actual output
E_D	Exergy destruction rate (kW)	$\hat{y}_i$	Predicted output
$f(x)$	Activation function	*Greek letters*	
F	Thrust force (kN)	ΔT	Different Temperature (K)
LHV	Lower heating value (MJ/kg)	α	Bypass ratio
G	Gradient on the current mini-batch	η	Efficiency
$\bar{H}$	Specific enthalpy (kJ/kg)	ρ	Flight air density (kg/m^3)
H	Flight altitude (m)	π	Pressure ratio
K	Specific heat ratio	*Subscripts*	
$L(w)$	Loss function	0	Ambient
$\mathrm{m_t}$	First moment	ac	Cold stream
m	Mass flow rate (kg/s)	ah	Hot stream
M_w	Mass weight (g/mol)	av	Average
Ma	Flight-Mach number	a	Airflow
MAE	Mean absolute error	CC	Combustion chamber
MAPE	Mean absolute percentage error	c	Compressor
MSE	Mean Squared Error	d	Diffuser
N	Number of the samples	fan	Fan
P	Pressure (kPa)	f	Fuel
R	Correlation factor	ex	Exergy
R^2	Determination factor	HPT	High-pressure turbine
RMSE	Root mean square error	LPT	Low-pressure turbine
R_u	Global constant gas (J/kgK)	$mixer$	Mixer
$\bar{S}$	Specific entropy (kJ/kgK)	n	Nozzle
TSF	Specific thrust (Ns/kg)	NOx	Nitrogen oxides
TSFC	Thrust-specific fuel consumption (g/KNs)	P	Propulsive
T	Temperature (K)	th	Thermal
v_t	Second moment	$total$	Total
V	Velocity (m/s)	T	Turbine

1. Introduction

Gas turbines (GT) are one of the power generation cycle types that is an internal combustion engine (ICE) of a rotary machine. These engines operate on the Brayton cycle (BC). Classically, the GTs have extensive applications in various industries ranging from oil, gas, and petrochemicals to power generation plants and various propulsion systems like airplane propulsion structures. The simplest aero-GT engine configuration is Turbojet. The power turbine supplies the mechanical power required by the compressor. The emission gases generated from the fuel combustion and air after exiting the turbine are reflected in the nozzle. Accordingly, the flow velocity increases, then it depletes to the ambient. One of the most essential aero gas turbine engine types is the turbofan engine. The internal flow is separated into two fragments: the hot flow and the bypass flow in the turbofan engines. Turbofan engines are divided into two types: twin-spool, and three-spool. Correspondingly, turbofan engines syndicate bypass flow as cold flow, and turbojet as the hot core [1, 2]. Another division of turbofan engines includes two types: the mixed-flow turbofan engine and unmixed-flow turbofan jet engine. In mixed turbofan, the fuel combustion products go into a high-pressure turbine (HPT) and then push through the low-pressure turbine (LPT) after crossing HPT. So, the output flow enters from the low-pressure turbine to the mixer, and it combines with the bypass flow or fan output flow. Subsequently, the mixer output flow arrives at the nozzle. Finally, it exhausts in the ambient.

Recently, many studies have been done to improve turbofan engine performance. For example, Balli et al. [3] examined performance parameters, environmental sensitivity, and sustainability of the TF33 turbofan engine exploited widely in military aviation. In their investigation, valuation parameters including energy efficiency, exergy destruction ratio, fuel heating value ratio (FHVR), specific fuel consumption (SFC), and thrust were considered. Chen et al. [4] numerically investigated a turbofan with an inlet ejector nozzle fortified with a supplementary inlet door. This supplement has been used in the inlet bypass flow to ejector the nozzle. It increased the engine installed thrust. Also, the ejector nozzle model is applied to analyze the performance of its effect on the engine. Moreover, a prediction method has been proposed for the exhaust system of backward infrared radiation intensity prediction. The results indicated that the turbofan engine with an inlet ejector not only decreases the infrared radiation and specific fuel consumption compared to the conventional turbofan engine but also improved significantly the engine installed

thrust. Xu et al. [5] evaluated a new mixed-flow turbofan and called a novel re-cooled mixed-flow turbofan cycle (RMTC). It has been used for military aero-engine with a high thrust-weight ratio. Their investigation indicated that the specific thrust has been improved by increasing the outer fan flow temperature. Similarly, the turbine cooling air consumption can be concentrated by reducing the inner fan flow temperature during the compression process by adding a re-cooler. Also, they investigated the effects of bypass ratio on the specific thrust, fuel consumption rate, and re-cooler location on the RMTC performances in the applicable fight conditions. The parametric studies approved that the specific thrust enhancement of RMTC is more substantial at high flight-Mach number. Finally, the calculation results confirmed that the considered RMTC system proves potential application for high-speed military aircraft. Rao et al. [6] studied to improve the propulsive efficiency of a civil aero-engine design aimed at lowering specific thrust and idle descent conditions by swelling the bypass ratio. Also, the bypass ratio of discharge and core nozzles of a high-bypass ratio aero-engine have been studied in isolation and installed on an airframe. The results were showed that the supreme alteration in the bypass nozzle discharge coefficient between the installed and isolated aero-engine across the descent phase is $\simeq$1.6%. Bali and Caliskan [7] examined the JT15D turbofan engine and its components based on the energy, exergy, environmental, aviation, and sustainability analysis. They calculated the specific fuel consumption, the energetic efficiency, and the exergetic efficiency with amounts of 15.8 g/kN.s, 21.15%, 19.919%, respectively. Balli et al. [8] thermodynamically analyzed the TF33 turbofan engine with hydrogen fuel with conflicting kerosene fuel. The results showed that the fuel mass flow rate, the specific fuel consumption, energy efficiency, and thermal limit ratio were decreased by 63.83%, 60.61%, 0.757%, and 1.55%, respectively. In another study, Akdeniz and Balli [9] analyzed energy, exergy, and sustainability analysis for the PW4056 turbofan engine and its main components to detect the different fuel impacts at the same dead state conditions. They understood that the amount of fuel mass flow and the exhaust gases mass flow of the hydrogen fuel is lower than the kerosene fuel with the value of 1.03 kg/s, and 2.85 kg/s for the hydrogen fuel and 117.14 kg/s, and 118.96 kg/s for the kerosene fuel, respectively. In both cases, the minimum exergy efficient component was calculated at 64.24 % in the combustion chamber for the kerosene case and 58.20 % for the hydrogen case. The lowest relative exergy loss ratio was determined to be 28.28 % for fan outlet loss for hydrogen case, even though the maximum relative exergy

consumption ratio was determined to be 51.93 % for the combustion chamber in the case of hydrogen as fuel.

Thermodynamic analysis of gas turbines is done to evaluate the performance of engines by design variables. In this regard, Ibrahim et al. [10] proposed energetic and exergetic analysis of a gas turbine plant cycle. They evaluated the effect of exergy flow, inlet flow, and outlet flow of compressor, turbine, and combustion chamber in terms of physical exergy and chemical exergy. Their results showed that the highest exergy destruction rate was associated with the combustion chamber. In another investigation, Zhao et al. [11] analyzed the first and second laws of thermodynamics analysis for intercooled turbofan engines (ITE) under different working conditions. Their results showed that the highest exergy destruction between engine components is in the combustion chamber. Also, the intercooler method is a cause of exergy destruction decreasing in the combustion chamber. Aygun and Turan [12] studied the exergy performance of the gas turbine variable cycles for the next-generation combat aircraft. Also, considering the bypass ratio and the input temperature of the turbine as design variables, optimization performed using a genetic algorithm to maximize fuel consumption. They calculated the lowest possible amount of fuel consumption as 17.41 grams per second.

Najjar and Balawneh [13] thermodynamically analyzed and optimized turbojet propulsion as one of the GT types. In their study, the special thrust is strongly dependent on turbine inlet temperature (TIT). So, a 10 percent reduction in TIT leads to a 6.7% reduction of the specific thrust and a 6.8% reduction in specific fuel consumption. It is also the optimal value for the turbojet parameters in the flight altitude condition of 13,000 meters and the Mach number of 0.8 with the compression ratio of 14 and TIT of 1700 K. Also, Hendricks and Gray [14] produced a new tool for analyzing and optimizing the thermodynamics performance of GT-cycles. They called the device as pyCycle. The code can compute the data of thermodynamic cycles at a rate of 0.03 % compared to the results obtained by the NPSS program. In another study, Xue et al. [15] studied the effects of bypass ratio in the optimal compression ratio of fan in the Trent-XBW engine series. It showed that the bypass factor is a cause of more effective in reducing fuel consumption and increasing the thrust force.

Previous studies show that the heat value of fuel affects the performance of gas turbine engines. Also, the specific chemical exergy and the heat value of the fuel are effective in the exergetic operation of gas turbine engines. In recent studies, the effect of the use of Hydrogen fuel compared

to hydrocarbon fuels on the performance of gas turbine engines has been investigated. Balli et al. [16] investigated the effect of using hydrogen fuel on the exergetic performance of a turbojet engine. Their results showed that with hydrogen fuel compared to hydrocarbon fuels, the exergy efficiency was reduced from 15.40% to 14.33 %. In another study, Gaspar and Souca [17] considered the effects of different fuels on the functional performance and environmental performance of a small turbofan engine. Also, the performance and intensity of ecological performance were investigated in the different working conditions. Verstraete [18] compared the action of the fueled hydrocarbon and fueled kerosene of long-range aircraft. Using hydrogen as fuel compared to the utilization of kerosene fuel, the direct operating cost and energy consumption have decreased by 3 and 11 %, respectively. Derakhshandeh et al. [19] simulated and optimized the environmental analysis and economic analysis of the GE90 turbofan engine. In their study, a comparison between hydrocarbon fuels and hydrogen fuels was performed on design conditions. In Hydrogen fuel, the GE90 turbofan engine economically and environmentally has been optimized. Their results showed that the optimized cycle increased the thrust force and thermal efficiency by 16.27% and 2.65 %, respectively by using Hydrogen fuel. Also, propulsive efficiency and overall efficiency decreased by 2% and 2.5%, respectively.

Recent studies indicate that the variation of the input temperature affects on performance of gas turbine engines. The variation of air temperature changes causes the variation of the incoming air density and changes in the inlet airflow to the engine. Changes in the inlet air temperature on the engine cause the switching performance parameters and exergy efficiency of gas turbine engines. Also, Caposciutti et al. [20] studied the effect of ambient temperature variations on the performance of a gas turbine plant with biogas fuel. In their study, by reducing the input temperature, the power plant increased 4.5%. In addition, due to the operational advantages of flying at high altitudes, it is crucial to assess the challenges of the gas turbine engine cycle in high altitude flight conditions. In the study of Treuren and McClain [21], the values found in the fan pressure ratio and the bypass ratio for a turbofan engine are engines designed to fly at 65,000 feet above sea level. The fan pressure, compressor pressure, and bypass ratio have been calculated at 1.57, 16.7, and 5.45, respectively.

2. Literature Review

The importance of reviewing gas turbine engines studies by using different Machine learning (ML) methods [22] specially supervised learning approach [23] can be shown in the literature. In this regard, many studies are worked on the aero-system based on intelligent systems. For example, Park et al. [24] using an artificial neural network (ANN) predicted the operating features of a gas turbine combustor. They utilized real-time data from industrial gas turbines with design parameters including the turbine exhaust temperature, fuel mass flow, turbine inlet temperature, fuel distribution of each nozzle, NOx, operating pressure of combustor, and inlet air temperature of the combustor. The root mean square error did not show a stable trend, which indicates the need for a failure sensor to adjust the sensitivity analysis. Also, they state that when there was a sudden change in operation in a short time, the prediction error highly increased.

Kaba et al. [25] intensely enhanced performance of civil and military aircraft engines using an improved least-squares estimation-based genetic algorithm (LSEGA) in fight phases. The thrust, SFC, and overall and exergy efficiencies are considered as parametric studies. They observed that the obtained model is successful in predicting all the considered thermodynamic parameters, so that the root mean square error for overall efficiency, exergy efficiency, SFC and thrust is 0.000311, 0.000162, 0.0763, and 1.007, respectively. Eventually, they observed that the LSEGA algorithm has effectively converged into optimal solutions for all indexes, and flight conditions with high accuracy. Orozco et al. [26] using artificial neural networks, proposed a diagnostic system for externally fired gas turbines to detect inherent defects and the impact of the fuel. They showed whether a heating system operates at its optimum level or requires an optimization process. Giorgi and Quarta [27] used different machine learning techniques to estimate behavior of turbojet engine based on the Viper 632-43 engine regarding the exhaust gas temperature (EGT) as the key parameter. The EGT estimated by A multigene genetic programming (MGGP) technique, which was added to the one-step-ahead EGT prediction data set. This structure was able to predict the output in the next time step as a real-time series.

Wang et al. [28] used semi-supervised deep learning method to estimate the remaining useful life (RUL) for reduce maintenance costs and develop maintenance strategies. They proposed a novel concurrent semi-supervised model (NCSS) to estimate the RUL of the aero-engine. The NCSS could be provided satisfying prediction results with only a small amount of labeled data. The experimental fallouts indicated that the considered method was operative in the commission of

RUL. Zhou et al. [29] utilized convolution neural networks (CNN) and recurrent neural networks (RNN) to fault diagnosis of gas turbine. They stated that the accuracy of CNN is better than RNN, in which the original CNN accuracy was 91.10%. Talaat et al. [30] using artificial neural network, proposed an intelligent model to predict the deterioration of a power plant gas turbine for main engine components such as compressor, combustion chamber, and turbine. The neural network model is trained using the deterioration data obtained from the thermodynamic model. The optimal structure including the number of hidden layers, the number of neurons in these layers and the transfer function is attained with the aim of minimizing the mean square error. Also, the dissimilar deterioration data as testing data was produced in thermodynamic analysis to test the efficacy of the neural network.

Zhou et al. [31] used Hopfield neural network based generalized predictive control strategy to optimize the performance of the turbofan engine. Using self-adaptive and identification modules, they designed an optimal controller. The results authorized the satisfactory performance of the proposed approach at the designated points and conditions rather than old-style algorithms. Also, the computer calculation time is significantly reduced. Tian et al. [32] proposed a maximum entropy reinforcement learning framework and the constrained Lyapunov-based actor-critic algorithm for an instantaneous model calibration. They suggested a novel framework for the inference of model parameters based on reinforcement deep learning to evaluate two dissimilar turbofan engines. Their experimental results demonstrated that the projected methodology outperformed all other verified methods in terms of speed and robustness, with high inference accuracy.

The above literature review shows that, while there exists a large body of literature studying the thermodynamic analysis of gas turbine engines, it appears that a comprehensive investigation has not been considered on the F135 PW100 engine. Accordingly, in the present study, for the first time, the effects of flight-Mach number, flight altitude, fuel types, and intake air temperature on thrust specific fuel consumption, thrust, intake air mass flow rate, thermal and propulsive efficiencies, the exergetic efficiency, and the exergy destruction rate in F135 PW100 engine are investigated. Moreover, based on the results obtained in the first part, a deep neural model for predicting the thrust, thrust specific fuel consumption (TSFC), and overall exergetic efficiency is attained based on the deep learning approach.

3. Problem description and modeling

3.1. Energy and exergy modeling

A schematic of the dual spools mixed-flow turbofan engine configuration with an inlet air cooling system illustrates in Fig. 1. In this system, the input airflow is driven into the fan from the inlet air cooling system. A portion of the fan output flow enters the bypass channel and enters the mixer. The other part of the fan output flow enters into a high-pressure compressor (HPC). The HPC output flow enters the combustion chamber (CC), and the air reacts with fuel in the CC. Subsequently, the flow of air combustion products with fuel enters a high-pressure turbine and drives it. The output flow of the high-pressure turbine enters the lower pressure turbine and then enters the mixer. Subsequently, the bypass channel output flow and the output flow of the LPT are combined in the mixer. Then the mixer output flow is produced by the nozzle; finally, it exhausts to the ambient.

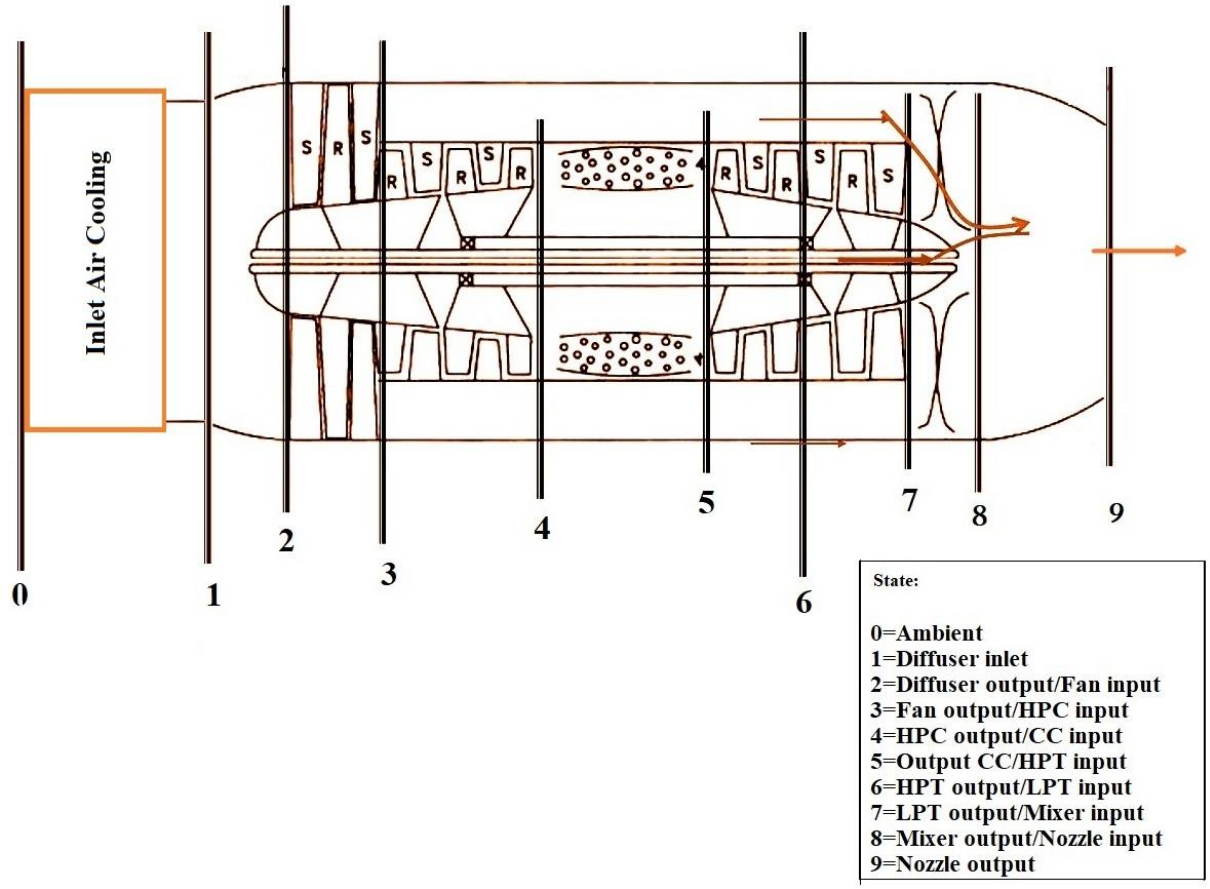

Fig. 1. Schematic of the dual spools mixed-flow turbofan engine configuration with inlet air cooling system.

The Governing energy analysis of this study is presented as follows. The changes in airflow pressure at the intake and cooling system are negligible, so the diffuser inlet pressure equals ambient air pressure ($P_0 = P_1$). Also, the inlet temperature can be calculated as;

$$T_1 = T_0 + \Delta T \tag{1}$$

where T_0 and ΔT are ambient air temperature, and difference inlet temperature, respectively. Assuming the diffuser is isentropic, the diffuser exit air temperature is calculated as follows;

$$T_2 = T_1\left(1 + \frac{k_d - 1}{2} M_a^2\right) \tag{2}$$

where T_1 and T_2 are respectively inlet and exit air temperature to the diffuser, M_a is the flight Mach number, and k_d is the diffuser specific heat ratio defined as specific heat at constant pressure to specific heat in constant volume for air passing through the diffuser.

The output air pressure of the diffuser is calculated as follows;

$$P_2 = P_1\left(\frac{T_2}{T_1}\right)^{\frac{k_d}{k_d - 1}} \tag{3}$$

where P_1 and P_2 are air pressure at the inlet and exit of the diffuser, respectively, and T_1 and T_2 are inlet and exit air temperature to the diffuser. Assuming air and fuel combustion products with air are ideal gas, the fan output pressure is obtained from the following equation.

$$P_3 = \pi_{fan} P_2 \tag{4}$$

where π_{fan} is the fan pressure ratio, P_3 is the fan exit air pressure, and P_2 is the fan inlet air pressure. Also, fan output air temperature is calculated as follows;

$$T_3 = \frac{T_2}{\eta_{fan}}\left[\left(\frac{P_3}{P_2}\right)^{\frac{k_{fan} - 1}{k_{fan}}} - 1\right] + T_2 \tag{5}$$

where η_{fan} is the fan isentropic efficiency, T_2 is the fan inlet air temperature, and K_{fan} is the specific heat at constant pressure to specific heat in constant volume for the passing air, which is calculated as a function of the average temperature of the passing air. Output air pressure of HPC is obtained as follows;

$$P_4 = \pi_c P_3 \tag{6}$$

where π_c is the compressor pressure ratio of HPC, P_4 is HPC output pressure, and P_3 is the fan exit air pressure. the exit temperature of the compressor is obtained as follows;

$$T_4 = \frac{T_3}{\eta_C}\left[\left(\frac{P_4}{P_3}\right)^{\frac{k_c-1}{k_c}} - 1\right] + T_3 \tag{7}$$

where η_c is the HPC isentropic efficiency, T_4 is HPC output air temperature, $T_3$is the fan output air temperature, and K_c is the specific heat at constant pressure to specific heat in constant volume for passing air of HPC is calculated as a function of the average air passing temperature of the HPC. Engine intake air real mass flow rate is calculated as follows;

$$m_{total} = \rho V_0 A \tag{8}$$

where A is a cross-section of an air inlet flow, ρ is the density of inlet airflow, and V_0 is flight velocity. The hot stream real air mass flow rate is obtained as follows;

$$m_{ah} = \frac{m_{total}}{\alpha + 1} \tag{9}$$

where m_{total} is engine intake air real mass flow rate, and m_{ah} is hot stream real air mass flow rate of engine core. Compressor power is obtained as follows;

$$W_c = m_{ah} Cp_3 \frac{T_3}{\eta_c}\left[\left(\frac{P_4}{P_3}\right)^{\frac{k_c-1}{k_c}} - 1\right] \tag{10}$$

where W_C, m_{ah}, η_c, and Cp_3 are HPC power consumption, hot-stream air mass flow rate, HPC isentropic efficiency, and the specific heat at a constant pressure of the HPC, respectively. Also, K_c is the ratio of specific heat in constant pressure to specific heat at constant volume in the HPC. Notably, both Cp_3 and K_c are calculated as a function of the average air passing temperature of the HPC. fan power consumption is obtained as follows;

$$W_{fan} = m_{total} Cp_2 \frac{T_2}{\eta_{fan}}\left[\left(\frac{P_3}{P_2}\right)^{\frac{k_{fan}-1}{k_{fan}}} - 1\right] \tag{11}$$

where W_{fan}, η_{fan}, and Cp_2 are fan power consumption, fan isentropic efficiency, and the specific heat at a constant pressure of fan, respectively. Also, m_{ac} is bypass air mass flow rate, and K_{fan} is the ratio of specific heat at constant pressure to specific heat to constant volume and specific heat at constant pressure, which is calculated as a function of the average fan air temperature.

$$m_{ac} = m_{total} - m_{ah} \tag{12}$$

where m_{ac} is bypass real mass flow rate and m_{ah} is hot stream real air mass flow rate of engine core.

Combustion chamber output pressure is obtained as follows;

$$P_5 = P_4 - \Delta P_{CC} \tag{13}$$

where P_5 is the CC output pressure, and P_4 is the compressor inlet pressure. Also, ΔP_{CC} is a pressure drop in the combustion chamber, which is evaluated as a percentage of the air exit pressure of the compressor. The heat transfer rate is calculated as follows;

$$Q_h = m_{ah} C_{av,cc} (T_5 - T_4) \tag{14}$$

where Q_h is heat rate, and $C_{av,cc}$ is the specific heat at constant pressure which is calculated as a function of average flow temperature in the combustion chamber. Also T_4 is the inlet air temperature of combustion chamber, and T_5 is the high-pressure turbine input air temperature. Accordingly, the fuel mass flow rate is calculated as follows;

$$m_f = \frac{Q_h}{LHV_f \eta_{CC}} \tag{15}$$

where LHV_f is the fuel's low heat value per kilograms, η_{CC} is combustion efficiency at the combustion chamber, m_f is fuel consumption, and Q_h is heat rate. Turbine intake mass flow rate is calculated as follows;

$$m_T = m_{ah} + m_f \tag{16}$$

where m_f is fuel consumption rate, and m_{ah} is hot stream real air mass flow rate.

HPT power is calculated as follows;

$$W_{HPT} = m_T C_{Pav,HPT}(T_5 - T_6) \quad (17)$$

where m_T is HPT inlet mass flow rate, and $C_{Pav,HPT}$ is the specific heat at constant pressure which is obtained as a function of the average temperature in the high-pressure turbine. low-pressure turbine power is calculated as follows;

$$W_{LPT} = m_T C_{Pav,LPT}(T_6 - T_7) \quad (18)$$

where m_T is turbine inlet mass flow rate, and $C_{Pav,LPT}$ is the specific heat at constant pressure which is obtained as a function of the average temperature in the low-pressure turbine. Assuming that mechanical power losses in the spools are negligible, the high-pressure turbine power is equal to the high-pressure compressor power according to the energy conservation law;

$$m_T . C_{Pav,HPT} . (T_5 - T_6) = m_{ah} Cp_3 \frac{T_3}{\eta_C}\left[\left(\frac{P_4}{P_3}\right)^{\frac{k_c-1}{k_c}} - 1\right] \quad (19)$$

where T_6 is the HPT exit temperature, T_5 is the HPT inlet temperature, m_T is the HPT mass flow rate, η_c is the HPC isentropic efficiency.By obtaining the HPT output temperature of the equation (19), the turbine exit pressure is calculated as follows;

$$P_6 = P_5\left[1 - \frac{1}{\eta_{HPT}}\left(1 - \frac{T_6}{T_5}\right)\right]^{\frac{k_{HPT}}{k_{HPT}-1}} \quad (20)$$

where T_6 is the output temperature of the high-pressure turbine, T_5 is the inlet temperature of the HPT, P_6 is the HPT output pressure, and P_5 is the HPT inlet pressure. k_{HPT} is the ratio of specific heat at constant pressure to specific heat at constant volume, which is a function of the average temperature during the high-pressure turbine, and η_{LPT} is the LPT isentropic efficiency .Assuming that mechanical power losses in the spools are negligible, according to the energy conservation law, low-pressure turbine power is equal to Fan power.

$$m_T . C_{Pav,T} . (T_6 - T_7) = m_{ac} Cp_2 \frac{T_2}{\eta_{fan}}\left[\left(\frac{P_3}{P_2}\right)^{\frac{k_{fan}-1}{k_{fan}}} - 1\right] \quad (21)$$

where T_7 is the LPT exit temperature, T_6 is the LPT inlet temperature, m_T is the LPT mass flow rate, η_{fan} is the fan isentropic efficiency.

The low-pressure turbine exit pressure is calculated as follows;

$$P_7 = P_6\left[1 - \frac{1}{\eta_{LPT}}\left(1 - \frac{T_7}{T_6}\right)\right]^{\frac{k_{LPT}}{k_{LPT}-1}} \quad (22)$$

where T_7 is the output temperature of the low-pressure turbine, T_6 is the inlet temperature of the low-pressure turbine, and P_7 and P_6, respectively, are the LPT output pressure and LPT inlet pressure. k_{LPT} is the ratio of specific heat at constant pressure to specific heat at constant volume, which is a function of the average temperature during the low-pressure turbine, and η_{LPT} is the LPT isentropic efficiency.

Regardless of the temperature and pressure changes in the bypass duct, the flow temperature at the mixer output is calculated in such a way;

$$T_8 = \frac{T_7 C_{P7} m_{ah} + (m_{ac} C_{P3} T_3)}{C_{P7}} \quad (23)$$

where C_{P3} and C_{P7}, respectively, are a specific heat at constant pressure at fan and LPT output, which is calculated as a function of the flow temperature. Moreover, C_{P8} is the specific heat at constant pressure at nozzle input, K_n is the ratio of specific heat capacity at constant pressure to specific heat capacity at constant volume, which is calculated as a function of the average flow temperature at the nozzle, T_7 and T_8, respectively, are the flow temperature at the LPT output and the mixer output, m_{ac} is the cold-stream real air mass flow rate, and m_{ah} is the hot-stream real air mass flow rate. Assuming the ideal gas, the flow at the mixer outlet and the flow pressure at the mixer outlet (P_8) is calculated in such a way;

$$P_8 = \frac{1}{M_w}\rho R_u T_8 \quad (24)$$

where R_u and ρ are the gas global constant from the mass conservation law and airflow density, respectively. The output mixer mass flow rate (m_8) is the overall mass flow rates of air passing through the engine core, fuel flow rate, and cold stream air mass flow rate;

$$m_8 = m_{ah} + m_{ac} + m_f \quad (25)$$

where m_{ac}, m_{ah}, and m_f are, respectively mass of air passing through the cold path, the air passing flow through the engine core, and the fuel mass flow rate. The nozzle output pressure is calculated in such a way;

$$P_9 = P_8 \left[1 - \frac{1}{\eta_n}\left(1 - \left(\frac{T_9}{T_8}\right)\right)\right]^{\frac{K_n}{K_n - 1}} \tag{26}$$

T_9 and T_8, respectively, are the exit temperature and inlet temperature of the nozzle, η_n is the nozzle isentropic efficiency, P_8 and P_9, respectively, are the inlet pressure and exit pressure of the nozzle.The velocity of the flow at the nozzle output (V_9) is calculated in such a way;

$$V_9 = \left(2\eta_n \frac{K_n}{K_n - 1}\frac{R_u}{M_w} T_8 \left[1 - \left(\frac{P_9}{P_8}\right)^{\frac{K_n - 1}{K_n}}\right]\right)^{0.5} \tag{27}$$

where R_u and M_w are the gas global constant and molecular weight of combustion products, respectively. The thrust force of the engine is calculated in such a way [33];

$$F = m_8(V_9 - V_0) + A_9(P_9 - P_0) \tag{28}$$

where P_0 and V_0, respectively, are the ambient pressure and flight speed, A_9 is the area of the nozzle output section, F is the thrust force of the engine, and m_8 is the mixer exit mass flow rate. The specific fuel consumption is equal to the ratio of fuel mass flow rate to thrust force [33];

$$TSFC = \frac{m_f}{F} \tag{29}$$

Thermal efficiency (η_{th}) is calculated in such a way;

$$\eta_{th} = \frac{m_8(V_9^2 - V_0^2)}{2m_f LHV_f} \tag{30}$$

where m_8 is the mixer output mass flow rate. Propulsive efficiency (η_P) is calculated in such a way [33];

$$\eta_P = \frac{V_0 F}{m_8(V_9^2 - V_0^2)} \tag{31}$$

Exergy (Ex) is known as entropy-free energy (maximum amount of work) in each system [34]. Two types of exergies are defined in the thermodynamic analysis of the power generation cycles: the physical exergy and the chemical exergy. The physical exergy demonstrated the maximum workability that can be extracted from fluid flow and the chemical exergy designates the maximum work that can be extracted from fuel flow. Physical exergy of all engine components is premeditated for both inlet or outlet of airflow as;

$$e = (\bar{H} - \overline{H_0}) - T_0(\bar{S} - \bar{S_0}) \quad (32)$$

where $\bar{H}$, $\overline{H_0}$, $\bar{S}$, $\bar{S_0}$, and T_0 are respectively the specific entropy of the fluid flow, the specific entropy of the dead state, the specific enthalpy of the fluid flow, the specific enthalpy of the dead state, and the ambient air temperature. The exergy flow rate is equal to the generation of the air mass flow rate in the air-specific exhaust as follows [34];

$$Ex = m_a ex \quad (33)$$

where ex is the airflow physical exergy. Fuel flow chemical exergy rate is calculated as follows [35];

$$Ex_f = m_f ex_f \quad (34)$$

where m_f and ex_f are respectively, the fuel mass flow rate consumed by the engine, and the specific chemical exergy of the fuel. Specific chemical exergy of the hydrocarbon fuels is intended as follows [35];

$$ex_f = LHV_f(1.04224 + (0.011925\frac{a}{b}) - (\frac{0.042}{a})) \quad (35)$$

where LHV_f, a, and b are respectively the lower heating value of fuel, the number of carbon atoms in each fuel molecule, and hydrogen atoms in each fuel molecule. The overall exergetic efficiency of the turbofan engine is equal to the flight velocity multiplied by Thrust force to input fuel flow chemical exergy rate as [35];

$$\eta_{ex} = \frac{FV_o}{Ex_f} \quad (36)$$

The fan exergy efficiency is intended as follows [35];

$$\eta_{ex,fan} = \frac{E_3 - E_2}{W_{fan}} \tag{37}$$

where W_{fan}, E_3, and E_2 are respectively the fan mechanical power consumption, the output fan exergy rate, and the fan inlet exergy rate. The fan exergy destruction rate ($E_{D,fan}$) is written as [35];

$$E_{D,fan} = W_{fan} + E_2 - E_3 \tag{38}$$

Compressor exergetic efficiency is given as follows [35];

$$\eta_{ex,c} = \frac{E_4 - E_3}{W_c} \tag{39}$$

where E_4, E_3, and W_c are the compressor outlet flow exergy rate, the compressor inlet flow exergy rate, and the consumed mechanical power of the compressor, respectively. Correspondingly, the rate of exergy destruction in the compressor ($E_{D,c}$) is calculated as follows [35];

$$E_{D,c} = W_c + E_3 - E_4 \tag{40}$$

The high-pressure turbine exergy efficiency is calculated as [35];

$$\eta_{ex,HPT} = \frac{W_{HPT}}{E_5 - E_6} \tag{41}$$

where W_{HPT}, E_5, $\eta_{ex,HPT}$ and E_6 are respectively the turbine power output, the turbine exergy efficiency, the turbine input flow exergy rate, and the high-pressure turbine outlet flow exergy rate. Correspondingly, the turbine exergy destruction rate ($E_{D,HPT}$) is written as follows [35];

$$E_{D,HPT} = E_5 - E_6 - W_{HPT} \tag{42}$$

Low-pressure turbine exergy efficiency is calculated as [35];

$$\eta_{ex,LPT} = \frac{W_{LPT}}{E_6 - E_7} \tag{43}$$

where W_{LPT}, E_6, $\eta_{ex,LPT}$ and E_7 are respectively LPT power output, the LPT input flow exergy rate, the low-pressure turbine exergy efficiency, and the low-pressure turbine outlet flow exergy

rate. Correspondingly, the low-pressure turbine exergy destruction rate ($E_{D,LPT}$) is premeditated as follows [35];

$$E_{D,LPT} = E_6 - E_7 - W_{LPT} \tag{44}$$

Also, The combustion chamber exergy efficiency is intended in this way [35];

$$\eta_{ex,CC} = \frac{E_5}{E_4 - E_f} \tag{45}$$

where E_f, $\eta_{ex,CC}$, E_4, and E_5 are respectively the chemical fuel flow exergy rate, the combustor exergy efficiency, combustor input flow exergy rate, and output flow exergy rate. The exergy destruction rate is considered in the combustion chamber as ($E_{D,CC}$) as follows [35];

$$E_{D,CC} = E_4 - E_5 + E_f \tag{46}$$

Also, The mixer exergy efficiency is intended in this way [35];

$$\eta_{ex,mixer} = \frac{E_8}{E_3 + E_7} \tag{47}$$

where E_7, $\eta_{ex,mixer}$, E_3, and E_8 are respectively the LPT output flow exergy rate, the mixer exergy efficiency, fan output flow exergy rate, and the mixer output flow exergy rate. The exergy destruction rate is considered in the mixer as ($E_{D,mixer}$) as follows [35];

$$E_{D,mixer} = E_7 + E_3 - E_8 \tag{48}$$

Also, The nozzle exergy efficiency is intended in this way [35];

$$\eta_{ex,n} = \frac{E_9}{E_8} \tag{49}$$

where E_8, $\eta_{ex,n}$, E_9 are respectively the mixer output flow exergy rate, the nozzle exergy efficiency, nozzle output flow exergy rate. The exergy destruction rate is considered in the nozzle as ($E_{D,n}$) as follows [35];

$$E_{D,n} = E_8 - E_9 \tag{50}$$

3.2. Deep learning

The artificial neural network is a significant part of machine learning techniques that can be found in a large set of data inspired by the performance of the brain, i.e., approves practical implementation and optimized application in many aspects such as manufacturing, computer vision, engineering, robotics, emotional intelligence, natural language processing, etc. The ANN is mainly composed of three parts: the first part consists of an input layer; the middle section contains one layer or more multi-hidden layers, and the last part contains an output layer, which is shown in Fig. 2.

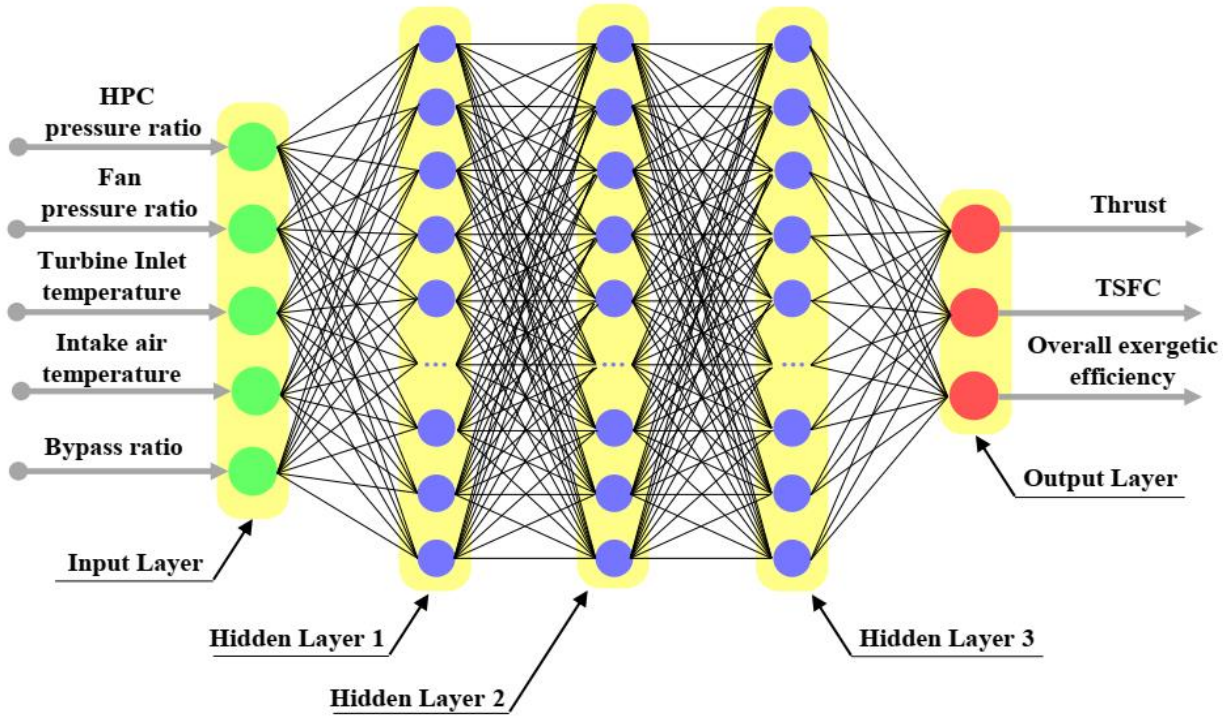

Fig. 2. Schematic of the deep neural network.

Deep learning is a kind of neural network that has several layers and significant neurons in the hidden and output parts. The present study has received the network, the data, and the parameters affecting the process, such as fan pressure ratio, HPC pressure ratio, variation of intake air temperature (IAT), TIT, and bypass ratio in the input layer and gives the results in the output layer after deciphering the hidden layers.

As shown in Fig. 2, hidden layer and output layers are composed of artificial neurons that have several weight coefficients and activation functions. The input values of each neuron are collected

together after a weighting process, and then the output of the neuron is calculated by the activation function. Activation functions as an example can be selected from among the Tanh, sigmoid, and rectified linear unit (Relu), which Relu has attracted much attention and is defined as follows;

$$f(x) = \begin{cases} xifx > 0 \\ 0ifx \leq 0 \end{cases} = \max(x, 0) \quad (51)$$

In the learning procedure of artificial neural networks, there are two basic approaches include, supervised learning and unsupervised learning. The first one, labeled data will help to predict outcomes while another one does not. In this study, such as many applications, we used a supervised approach where the output is compared with the actual output. In particular, the weight of the neuron is calculated in such a way that the predicted output in return for a series of inputs can be as close as possible. It should be noted that quantification of network error for approximation of the results is done using the cost function or loss function, one of the most common loss functions is mean squared error which is defined as follows;

$$L(y, \hat{y}) = \frac{1}{N}\sum_{i=1}^{N}(y_i - \hat{y}_i)^2 \quad (52)$$

where N is the number of samples, y_i is the actual output, and $\hat{y}_i$ is the predicted output. The mean squared error function is often used for deep neural networks with the objective of approximation continuous values (regression problems). As mentioned, in the learning process, the weight calculation of each neuron is considered to minimize the loss function. First-order optimization algorithms based on the gradient descent method are among the most popular methods for calculating the neuron's weight. If w is the weight vector of the network weights, the loss function $L(w)$ can be defined as;

$$L(w) = \frac{1}{N}L_i(w) \quad (53)$$

where L_i is the loss function of i-sampled and N is the number of the samples.

There are several optimization algorithms to minimize loss function, such as standard gradient descent, stochastic gradient descent (SGD), root mean square propagation (RMSProp), and adaptive moment optimization (ADAM), which the latter of them has received a lot of attention due to computational efficiency, simplification in implementation, short memory requirement, etc. Adam is considered as a combination of RMSProp and SGD methods with momentum because like RMSProp uses the square gradient to scale the learning rate and resembles the momentum

benefits from the moving gradient mean. Adam calculates the momentum as the weighted average of the gradients as follows:

$$m_t^{(j)} = \beta_1 m_{t-1}^{(j)} + (1-\beta_1) g_t^{(j)} \tag{54}$$

$$v_t^{(j)} = \beta_2 v_{t-1}^{(j)} + (1-\beta_2)(g_t^{(j)})^2 \tag{55}$$

where m_t is the first moment, v_t is the second moment, g is the gradient on the current mini-batch, and also $\beta_1$and β_2 are exponential decay rates respectively considered as 0.9 and 0.999. Then, the first moment and the second moment are bias-corrected as:

$$\widehat{m}_t^{(j)} = \frac{m_t^{(j)}}{1-\beta_1^t}, \hat{v}_t^{(j)} = \frac{v_t^{(j)}}{1-\beta_2^t} \tag{56}$$

Also, the updating of the weights is carried out according to the equations (57) with alpha learning which is assumed to be equal to 0.001.

$$w_{t+1}^{(j)} = w_t^{(j)} - \frac{\alpha}{\sqrt{\hat{v}_t^{(j)}} + \varepsilon} \widehat{m}_t^{(j)} \tag{57}$$

Using momentum instead of gradients to update neuron weights helps ADAM accelerate to find local minima.

3.3. Keras

Keras is an application program interface designed not only for machines but also for humans. Keras is an open-source programming platform that builds simple and compatible APIs, reduces the number of user actions, and provides practical and clear error messages. Keras can run various machine learning libraries such as Theano (developed by the University of Montreal), CNTK (designed by Microsoft), and TensorFlow (acquired by Google). Keras, which provides fast and easy prototyping with features of modularity, scalability, and user-friendliness, has been ranked second after TensorFlow in 2018 in the power ranking, which emphasizes popularity, and interest. In the Keras platform, which is programmed in Python, neural networks with different structures can be created. Also, in Keras, all activation functions, loss functions, and even optimization algorithms such as Adam, RMSProp and SGD are applicable. As a result, due to its widespread use and unique benefits, Keras has also been used in the Python context in this study.

4. Validation

The F135 PW100 turbofan engine is a mixed-flow turbofan. This engine is used as a propulsion system of the Lockhid Martin F-35 Lightning. The components of the F135 PW100 engine include an axial-flow fan with three stages, HPC with six stages, a combustion chamber, HPT with one stage, LPT with two stages, mixer, and nozzle [36]. The Input Parameters of the F135 PW100 engine are shown in Table 1 [36].

Table 1. Input parameters of F135PW100 engine modeling.

Parameters	Symbol	Value	Unit
Inlet air mass flow rate	m_a	147	Kg/s
Fan pressure ratio	π_{fan}	4.7	-
High-Compressor pressure ratio	π_c	6	-
Isentropic efficiency of the fan	η_{exc}	0.90	-
Isentropic efficiency of the high-pressure compressor	η_{exHPC}	0.85	
High-pressure turbine inlet temperature	TIT	2175	K
Isentropic efficiency of the high-pressure turbine	η_{exHPT}	0.90	-
Isentropic efficiency of the low-pressure turbine	η_{exLPT}	0.91	-
Isentropic efficiency of the combustion chamber	η_{exCC}	0.995	-
Bypass ratio	α	0.57	-

The efficacy of several fuel types, such as hydrogen fuel, and natural gas (LNG) has also been inspected on the performance of the proposed engine. The main component of LNG is methane, and residual components are ethane, propane, butane, and nitrogen [37], of which methane is a major part; so, it can be approximated as a pure methane fuel (CH_4) that Su et al. [38] similarly supposed. JP10 is a missile and aero engines well-known fuel because of its high energy storage and high-energy-density fuels [39, 40]. JP10, also known as Exo-tetrahydro dicyclopentadiene ($C_{10}H_{16}$), as a cyclic single-component hydrocarbon [41-43]. The lower heating value (LHV) and Special chemical exergy of these fuels are given in Table 2. According to equation (35), the special chemical exergy of hydrocarbons fuels can be calculated.

Table 2. The fuel lower heating value and special chemical exergy of fuels [44-46].

Fuel type	JP10	Diesel	LNG	Hydrogen
Special chemical exergy of fuels (MJ/Kg)	44.921	44.661	55.168	134.778
LHV (MJ/Kg)	42.1	42.740	49.736	118.429
Molecular Weight (g/mol)	136	167	16	2
Chemical Formula	$C_{10}H_{16}$	$C_{12}H_{23}$	CH_4	H_2

Particularly, the efficiency of fuel types, flight altitude, and intake temperature variation on the F135 PW100 mixed-flow turbofan engine is investigated in three validation cases. At first, the comparison was performed in the take-off conditions ($Ma = 0$, and $H = 0$) with Ref. values [36], which represented in Table 3. The validation was evaluated for the thrust, the fuel consumption mass flow rate, and TSFC. The comparison shows that the error is in the acceptable range, which indicates the accuracy of the model.

Table 3. The fuel lower heating value and special chemical exergy of fuels.

	Modeling results	Ref. [36]	Error
Thrust (KN)	118.580	125.903	-5.81%
TSFC(g/KNs)	26.43	25	5.72%
Fuel mass flow rate (Kg/s)	3.134	3.15	-0.5%

Second, the TSFC engine is compared with another turbofan engine known as F100 regarding flight altitude, which has been done by Aygun and Turan [12] shown in Fig. 3a. The comparison demonstrated that thrust is decreased by increasing flight altitude at both engines. Also, at near-flight altitudes of 20,000 m; both engines have the same thrust. This confirmed a good agreement for thrust validation. Third, comparison was achieved with experimental work of Gunasekar et al. [47] where the exergetic performance of a gas turbine were evaluated by using hydrogen as fuel. As depicted in Fig. 3b, the mean absolute percentage error was calculated as 9.70 %, which showed a good agreement for using hydrogen fuel validation.

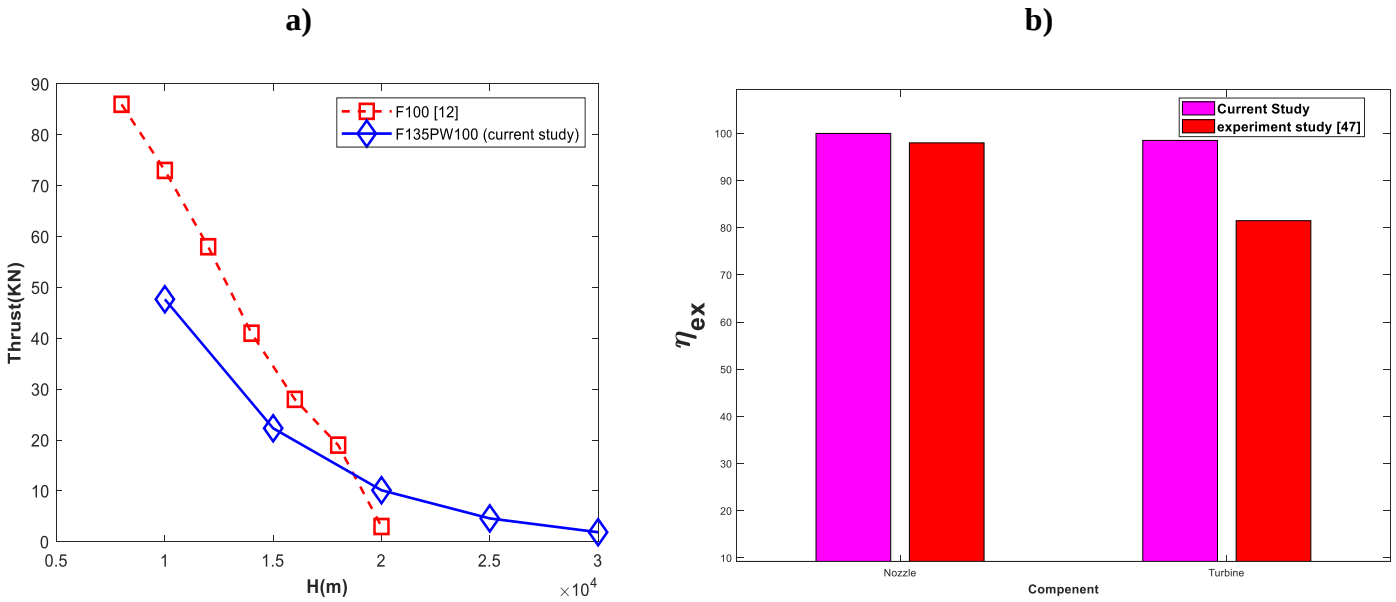

Fig. 3. Validation results a) based on thrust regarding flight altitude, and b) exergetic efficiency for nozzle and turbine.

5. Results and discussion

5.1. Engine performance analysis

5.1.1. Effect of Mach number and flight altitude on engine performance

In this subsection, the impact of Mach number and flight altitude on the intake air mass flow rate, TSFC, thrust, propulsive efficiency, and thermal efficiency of the F135 PW100 engine was investigated. Also, in this case, JP10 is used as fuel. The changes in intake air mass flow rate of the F135 PW100 engine with flight-Mach number and flight altitude are presented in Fig. 4a. It has been observed that the flight velocity increases at each constant flight height with increasing Mach number. Accordingly, the intake air mass flow rate to the engine increases as similar has been achieved in Ref. [48]. They evaluated the effect of flight-Mach number and flight altitude of turbofan engine on the intake air mass flow rate. Their results evidenced that the intake air mass flow increases at each flight altitude with increasing flight-Mach number [48].

Also, in each constant flight-Mach number, with increasing flight altitude, the intake mass flow rate to the engine decreases because the intake air density is reduced. Aygun and Turan [49] attempted to investigate the influence of flight-Mach number on the thrust in an aero- GT engine. They revealed that, with the higher flight-Mach number, there is an increase in the thrust force of

a gas turbine engine. The variation of the F135 PW100 engine thrust force with Mach number and flight altitude is represented by the use of JP10 fuel in Fig. 4b. At every constant flight height, with an increase in the flight-Mach number, intake airflow to the engine is increased, so the thrust force is increased as gotten in Ref. [50].

At each flight-Mach number, with increasing flight altitude, the mass flow entering the engine and consequently the thrust decreases. The variations of the thrust specific force (TSF) of the F135 engine are discussed at an altitude of 20,000 meters with flight-Mach using JP10 fuel in Fig. 4c. The modifications of the TSF of the F135 PW100 engine with flight altitude and flight-Mach number have been displayed in Fig. 4c by using JP10 fuel. The intake mass flow rate to the engine increases with increasing flight-Mach number at each constant flight height. Since with increasing flight Mach number, the intensity of the rising intake mass flow rate to the engine is higher than the intensity of the increase in the thrust, so TSF decreases with the increasing Mach number.

The TSFC changes of the F135 PW100 engine with flight height and Mach number have been displayed using JP10 fuel in Fig. 4d. By increasing the intake air mass flow rate to the engine, more energy is needed to reach the combustion chamber outlet temperature (limit of TIT). Therefore, the heating rate and fuel consumption mass flow rate increase with increasing the inlet air mass flow rate. The inlet air flow rate increases with flight-Mach number at each constant altitude. However, the rate of increase in fuel consumption mass flow rate is higher than that of the thrust. The TSFC increases with increasing flight-Mach number due to the increase in the intake air mass flow as gotten in Ref. [49]. They also found that TSFC increases with flight-Mach number.

Changes in thermal efficiency of F135 PW100 with flight-Mach number and flight altitude are shown in Fig. 4e. The representation showed that at each constant flight height with increasing flight-Mach number in the range of 1 to 2, thermal efficiency increases, and with increasing flight-Mach number in the range of 2 to 2.5, thermal efficiency decreases. The variation of the propulsive efficiency is represented with flight-Mach number and altitude by using the JP10 fuel in Fig. 4f. Since the flight-Mach number increases, both the thrust of the F135 engine and flight velocity increase, and the propulsive efficiency increases with increasing Flight-Mach number in each constant flight altitude.

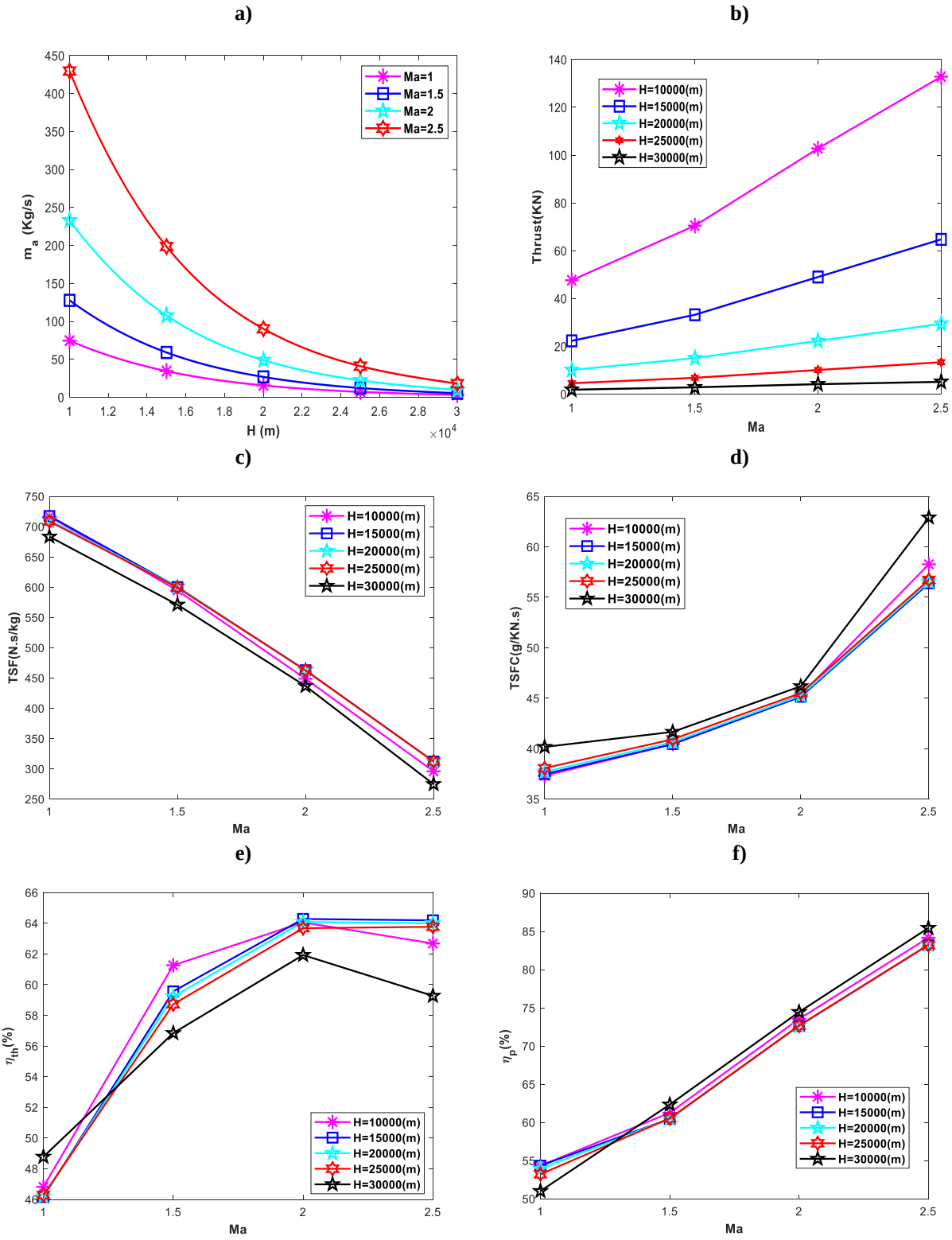

Fig. 4. The effects of Flight- Mach number and flight altitude of the F135 PW100 engine in a) the intake air mass flow rate, b) net thrust, c) TSF, d) TSFC, e) thermal efficiency, and f) thrust by using JP10 as fuel.

5.1.2. Effect of fuel types on engine performance

In present subsection, the effect of different fuels, including natural gas, hydrogen fuel, diesel fuel, and JP10 on performance parameters such as thrust, TSFC, thermal efficiency, and propulsive efficiency were investigated at the height of flight condition of 30,000 m altitude and Mach number of 2.5. Thrust force and TSFC changes are represented in Fig. 5a and Fig. 5b, respectively. The changes are applied by the fuel types at an altitude of 30,000 m and Mach number of 2.5. However, as the molecular weight of the fuel decreases, molecular weight of the combustion productions also decreases, resulting in an increase in the nozzle output velocity. As a result, the velocity term of the Thrust force increases. So, the thermodynamic cycle has the highest thrust force by using hydrogen as fuel, as shown in Fig. 5a.

Also, the TSFC changes of the F135 PW100 engine with fuel type at a flight height of 30,000m and flight-Mach number of 2.5 are shown in Fig. 5b. Consequently, the fuel consumption mass flow rate is reduced by increasing the fuel's lower heating heat value (LHV_f). Accordingly, TSFC is reduced by increasing the LHV_f. Also, the thermal, propulsive, and overall efficiencies of the F135 PW100 engine are represented by the fuel type at a flight altitude of 30,000 m and Mach 2.5 in Fig. 5c. Reducing the molecular fuel weight increases the nozzle exit velocity and thrust force, which in turn increases the rate of change in the kinetic energy of the flow along the engine. Also, due to the fact that the rate of increase in thrust force is lower than the rate of changes in kinetic energy of flow, accordingly as the molecular fuel weight decreases, the propulsive efficiency decreases. Also, the exit nozzle velocity and variation of the kinetic energy rate is reduced, by

increasing the molecular fuel weight along the engine. Consequently, thermal efficiency decreases with increasing the molecular fuel weight. As a result, the hydrogen fuel has the lowest amounts of TSFC, similarly achieved in Ref. [50]. They observed that the use of hydrogen fuel instead of hydrocarbon, TSFC is reduced, which Fig. 5b confirmed it.

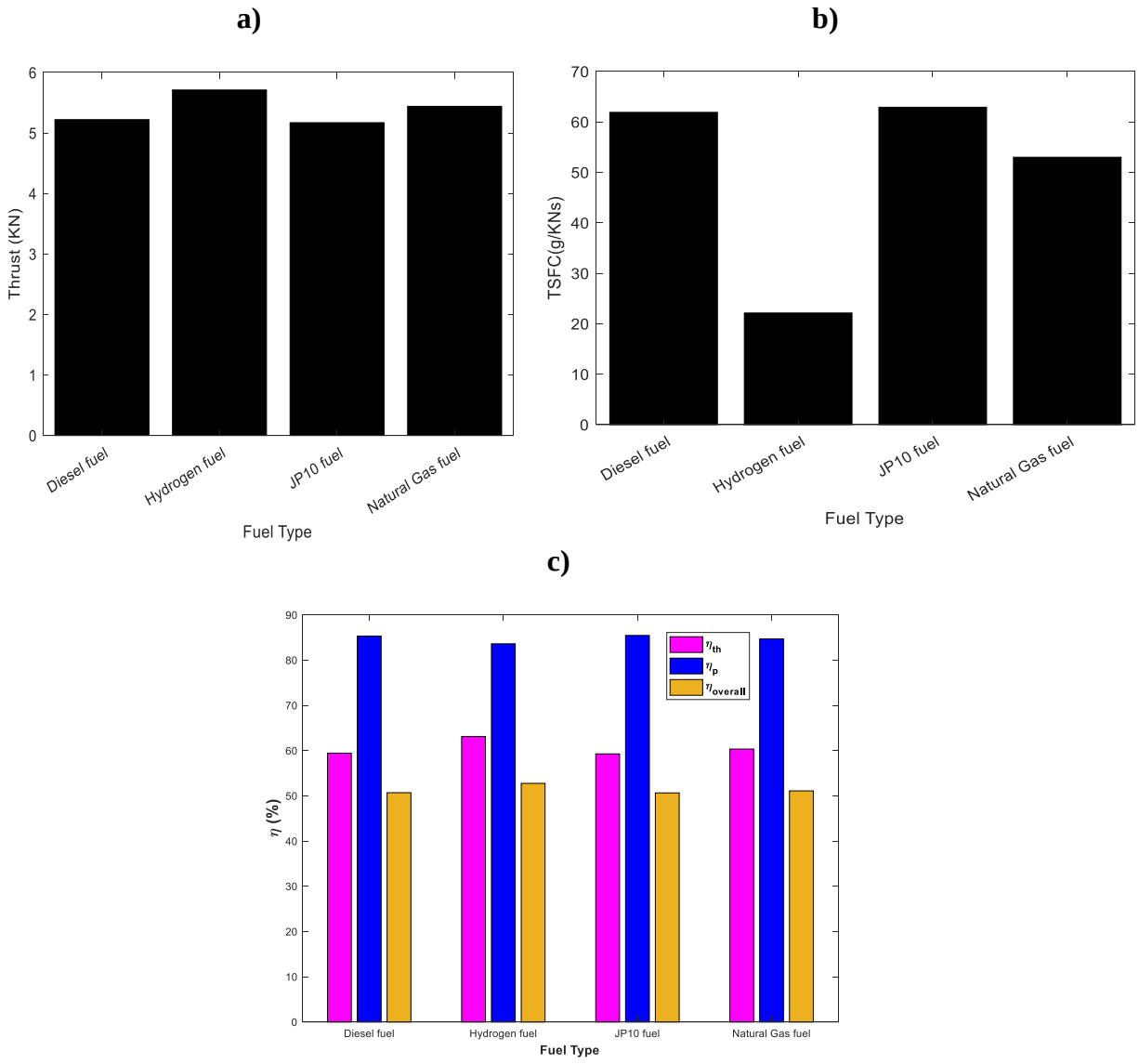

Fig. 5. The efficacy fuel type at an altitude of 30000m and flight-Mach number of 2.5 on a) TSFC, b) thrust force, and c) thermal efficiency, propulsive efficiency, and overall efficiency.

5.1.3. Effect of inlet air temperature changes on engine performance

In this subsection, the effect of intake air temperature variation on the thrust, TSFC, thermal efficiency, and propulsive efficiency of the F135 PW100 turbofan engine is investigated by using hydrogen fuel at different flight altitudes and flight-Mach numbers. Two fragments are disused: 1) flight-Mach number is assumed constant as 2 and flight altitude in the range of 10,000 m to 30,000 m; 2) The flight altitude is supposed constant as 20,000 m with varied flight-Mach number. These fragments are applied at three parameters.

First, the changes in inlet air mass flow rate of F135 PW100 in terms of the difference in inlet air temperature with different flight altitudes and flight-Mach numbers have shown in Fig. 6a and Fig. 6b. It has been observed that, at each flight altitude and Mach number, with decreasing inlet air temperature, the inlet air density increases, so the inlet air mass flow rate increases. Second, the changes in the thrust of the 135 PW100 engine with inlet air temperature are represented in Fig. 6c and Fig. 6d at different flight conditions. The intake air mass flow rate increases with decreasing the inlet air temperature in each flight condition . Subsequently, the thrust is increased.

Third, TSFC variation of the F135 PW100 engine is represented by decreasing inlet air temperature at different flight-Mach numbers and altitudes in Fig. 6e and Fig. 6f. In each case, reducing the intake air temperature requires more energy to deliver the flow temperature to the limit of TIT so the consumption fuel mass flow rate is increased.

However, as the intake air temperature decreases, the rate of increase in fuel consumption mass flow rate is greater than that of the thrust force, TSFC increases at an altitude of 20,000 m in the Mach number below 1. On the contrary, in the Mach number above 1, as the intake air temperature decreases, the rate of increase in fuel consumption mass flow rate is lower than that of the thrust force, TSFC is decreased at flight-Mach number of 2 and flight altitude in the range 10,000 m to 30,000 m. Also, the applied fragment is considered at the other performance parameters such as thermal efficiency, and propulsive efficiency.

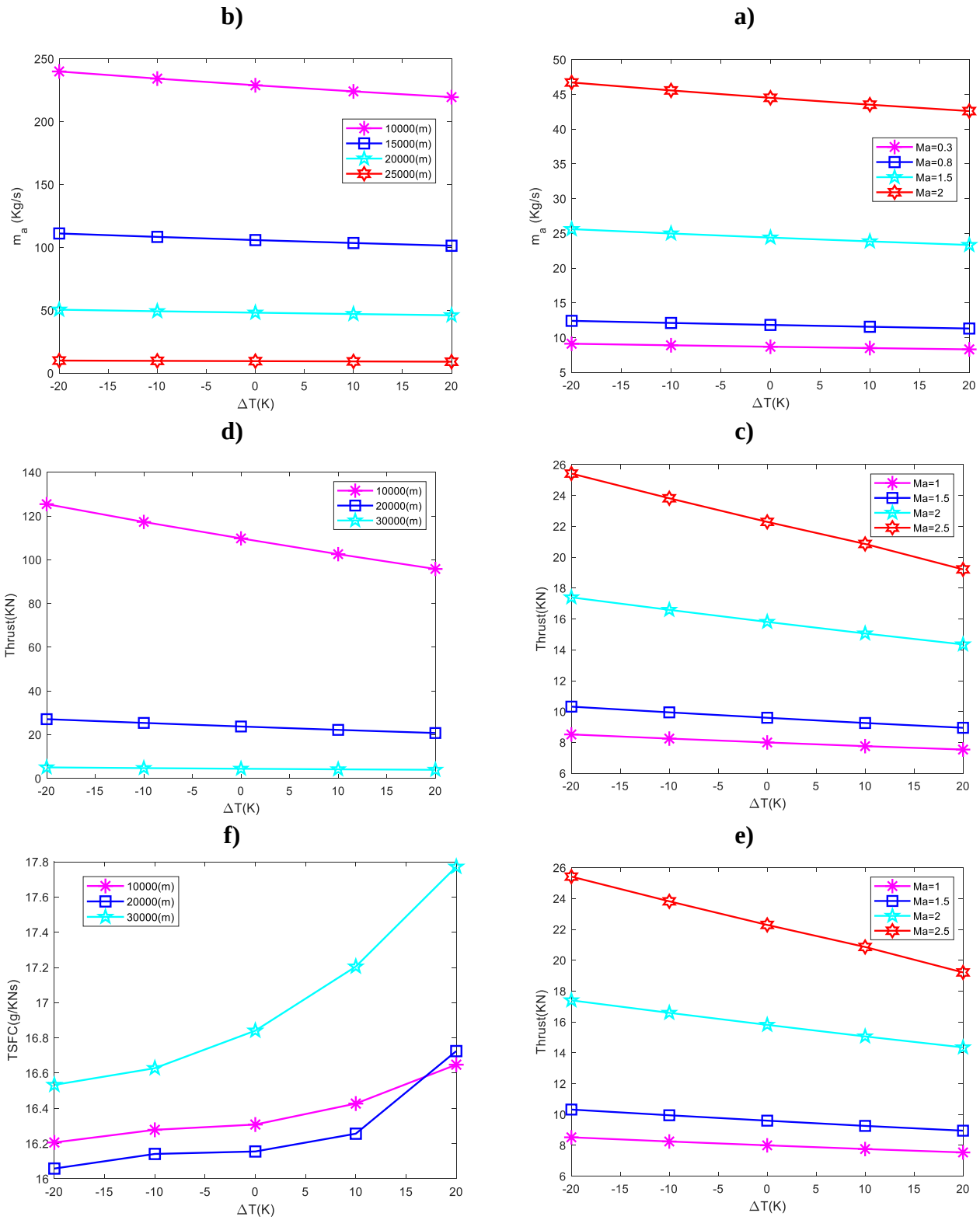

Fig. 6. The influences of difference inlet air temperature of the F135 PW100 engine with a) intake mass flow rate-varied flight altitude, b) intake mass flow rate-varied Flight-Mach number, c) thrust-varied flight altitude, d) thrust -varied flight-Mach number, e) TSFC-varied flight altitude, and d) TSFC -varied flight-Mach number.

The thermal efficiency variation of the F135 PW100 engine with decreasing intake air temperature at different flight-Mach numbers and flight altitudes is shown in Fig. 7a and Fig. 7b. In each flight case, the air mass flow rate increases by decreasing intake air temperature. Therefore, as the inlet air temperature decreases, the rate of change in the kinetic energy of the flow along the engine increases. Since the intensity of the increase in variation rate of the kinetic energy along the engine is higher than the intensity of the increase in heating rate due to the decreasing intake air temperature, the thermal efficiency increased with decreasing intake air temperature. Correspondingly, the change of propulsive efficiency is represented by reducing the temperature of the inlet air at flight-Mach number and the different heights in Fig. 7c and Fig. 7d.

The results showed that by decreasing the inlet air temperature, the kinetic energy of airflow to the engine increases. However, since the intensity rate of increase in the kinetic energy along with the engine is higher than the intensity of the increase in the thrust force due to the reduction in the intake air temperature, hence the input air temperature is reduced in any state, so it is the cause of decreasing in propulsive efficiency.

5.2. Exergy analysis results

5.2.1. Effect of Flight altitude and flight-Mach number

In this subsection, the exergy efficiency, and the exergy destruction rate of F135 engine components containing the fan, HPC, HPT, LPT, nozzle, and mixer are investigated by using JP10 as a fuel. In addition, the exergy efficiency and exergy destruction rate of the F135 PW100 engine with Mach number and altitude were analyzed by using JP10 as a fuel. The exergy efficiency and exergy destruction rate changes of the F135 PW100 engine and its components with changing the flight-Mach numbers and flight altitudes are indicated in Fig. 8a-d.

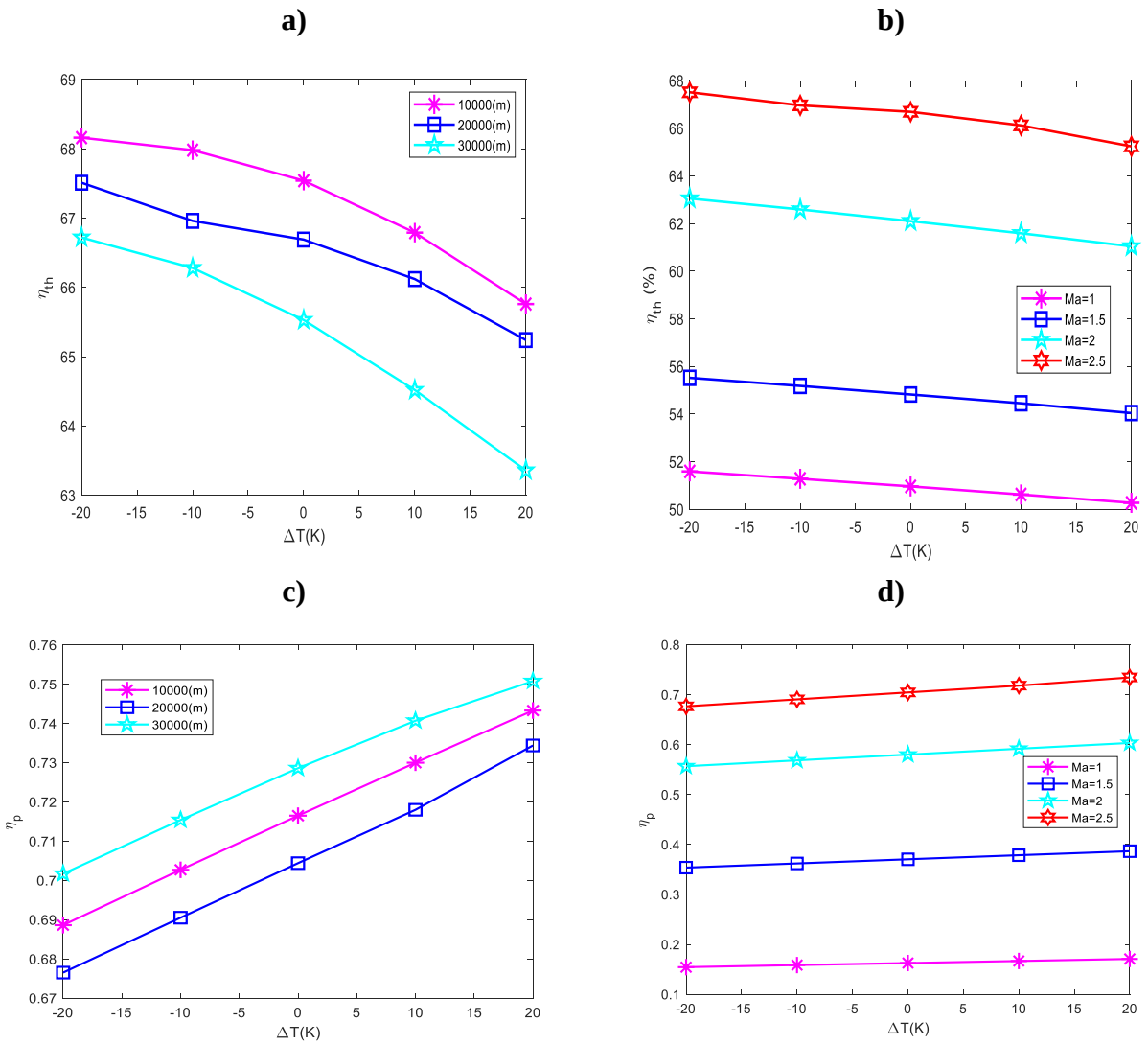

Fig. 7. The effects of the difference inlet air temperature of the F135 PW100 engine in terms of a) flight altitude variation in the range of 10,000 to 30,000 and constant flight-Mach number of 2 for thermal efficiency, b) flight-Mach number Variation and constant flight altitude of 20,000 m for thermal efficiency, c) flight altitude variation in the range of 10,000 to 30,000 and constant flight-Mach number of 2 for propulsive efficiency, and d) flight-Mach number Variation and constant flight altitude of 20,000 m for propulsive efficiency.

In Fig. 8a and Fig. 8c, the flight-Mach number is assumed as a constant amount of 2, and also, in Fig. 8b and Fig. 8d, the flight altitude is presumed as constant at 15000 m. Both, the mixer exergetic efficiency and the overall exergetic efficiency were increased by increasing the flight-Mach number at the constant flight altitude; similarly, recognized in Ref. [49]. They performed the efficacy of Flight Mach number on exergetic efficiency in GT engine. It has been demonstrated that exergetic efficiency is increased by increasing the flight-Mach number [49].

Also, the variation of the exergy destruction rate of the F135 PW100 engine and its components with Mach number and flight height is shown in Fig. 8c and Fig. 8d. The results exhibited that the exergy destruction rate of the components and overall exergy destruction rate of the F135 PW100 engine is decreased with increasing the flight altitude at constant flight-Mach number. Also, the exergy destruction rate of each component increases at the constant flight altitude by increasing the flight-Mach number.

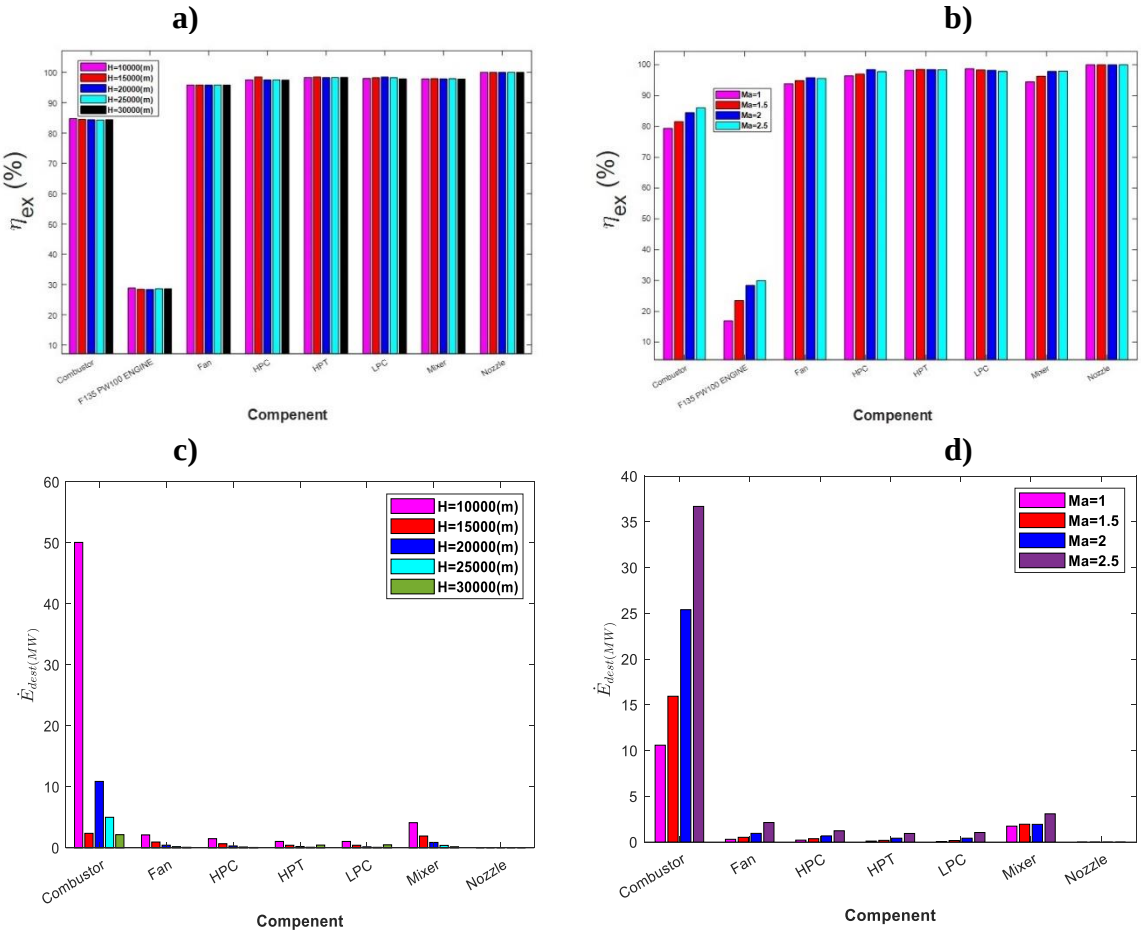

Fig. 8. Efficacy flight altitude and flight-Mach number of the F135 PW100 engine and its components a) exergetic efficiency with the constant flight-Mach number of 2, b) exergetic efficiency with a constant flight altitude of 15000 m, c) exergy destruction with constant flight-Mach number of 2, and d) exergy destruction with a constant flight altitude of 15000 m.

5.2.2. Effect of inlet air temperature changes

In this subsection, the effect of reducing the intake air temperature on the overall exergy efficiency of the F135 PW100 engine and F135 PW100's components including, HPC, HPT, LPT, fan, and mixer was investigated at an altitude of 20,000 m and Mach number of 2 by using JP10 as a fuel. Reducing the inlet air temperature is increased exergetic efficiency in flight conditions, which has been achieved in Ref. [51]. They investigated the effect of inlet air cooling on GT engine performance with different methods [51]. Their results proved that exergetic efficiency is increased when the inlet air temperature is reduced. In another study, Ibrahim et al. [10] showed that reducing of the inlet air temperature in open-GT engine increased exergetic efficiency.

The overall exergy efficiency changes of the F135 PW100 engine and its components with intake air temperature are indicated in Fig. 9a. The results evidenced that the overall exergy efficiency of F135 PW100, and exergy efficiency of HPT, LPT, HPC, and fan are increased by decreasing the intake air temperature. Moreover, the exergy efficiency of the combustion chamber and mixer is reduced by reducing the intake air temperature. Next, the changes in the overall exergy destruction rate of the F135 PW100 engine and components of F135 PW100 are indicated in Fig. 9b with intake air temperature changing at flight conditions of 20,000 m altitude and Mach number 2 by using JP10 as a fuel. The results confirmed that the exergy destruction rate of Fan, HPT, LPT, and HPC of F135 PW100 is reduced by reducing the intake air temperature. Consequently, the exergy destruction rate of the combustion chamber and mixer is increased.

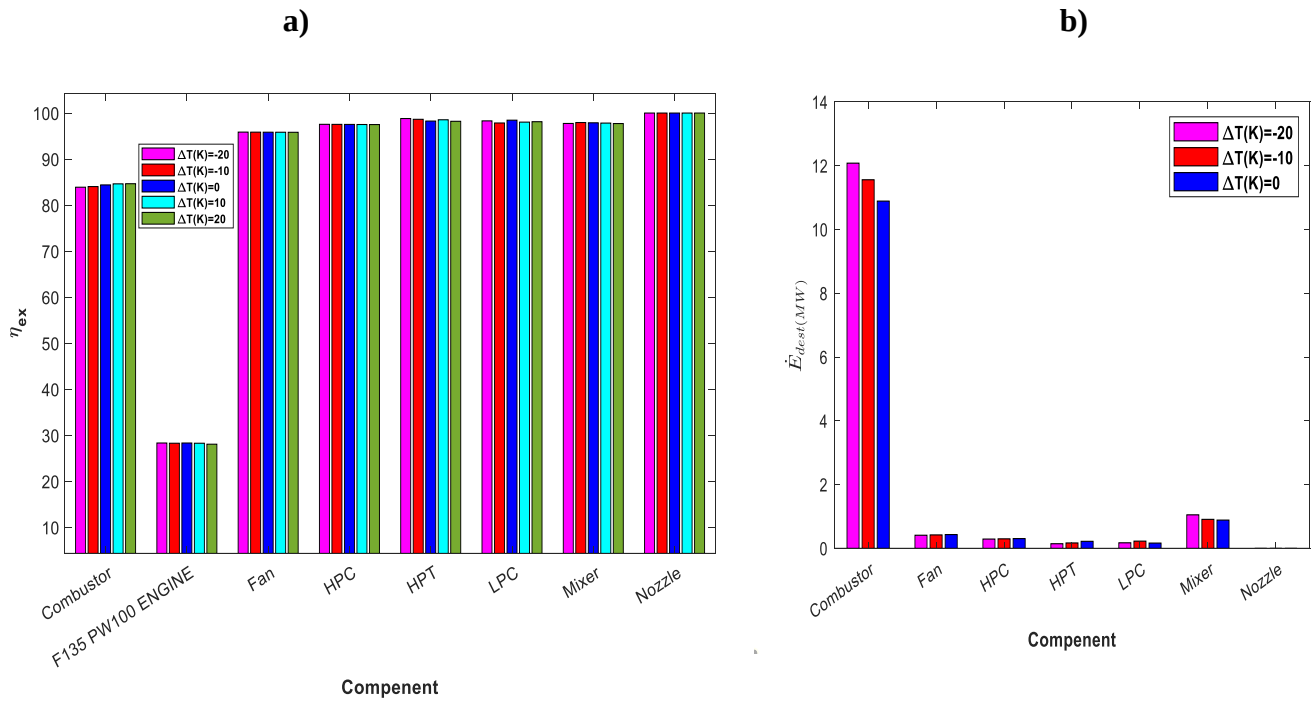

Fig. 9. The effects of difference inlet air temperature of the F135 PW100 engine and its components engine at a flight altitude of 20000 m and flight-Mach number of 2 via using JP10 fuel on a) exergetic efficiency, and b) exergy destruction.

5.2.3. Effect of fuel types

In this subsection, the exergy efficiency and exergy destruction rate of the F135 PW100 engine and its components of it including the HPC, HPT, LPT, and mixer at an altitude of 20,000 m and flight-Mach number of 2 are investigated by using hydrogen, natural gas and JP10 as fuels.

The exergy efficiency changes of the F135 PW100 engine and its components with the fuel type used at 20000 m altitude and flight-Mach number of 2 are shown in Fig. 10a. The results demonstrated that among the fuels, the JP10 has the maximum overall exergy efficiency, and the highest exergy efficiency. Also, Hydrogen fuel has the lowest overall exergy efficiency, and the lowest exergy efficiency achieved at the combustion chamber, which can be approved formerly in the gas turbine engines. For example, Gunasekar et al. [47] observed that with the use of hydrogen fuel instead of the Jet A-1 as a hydrocarbon fuel in turbojet engine, overall exergetic efficiency is

reduced by about 10 %. Also, Ibrahim et al. [10] verified that combustion chamber has the lowest exergetic efficiency and highest exergy destruction rate compared to other components.

Correspondingly, the effects of the exergy destruction rate of the F135 PW100 engine cycle and F135 PW100 engine's components with the different fuel types used at 20000 m altitude and Mach number of 2 are shown in Fig. 10b. The results demonstrated that the least exergy destruction rate is achieved by a nozzle with JP10. Also, the highest exergy destruction rate is produced by the combustion chamber with JP10. In the application of hydrogen fuel, the highest exergy destruction rate has occurred in all of the F135 PW100 engine's components. Also, the application of JP10 has the lowest exergy destruction rate of all of the components for the F135 PW100 engine.

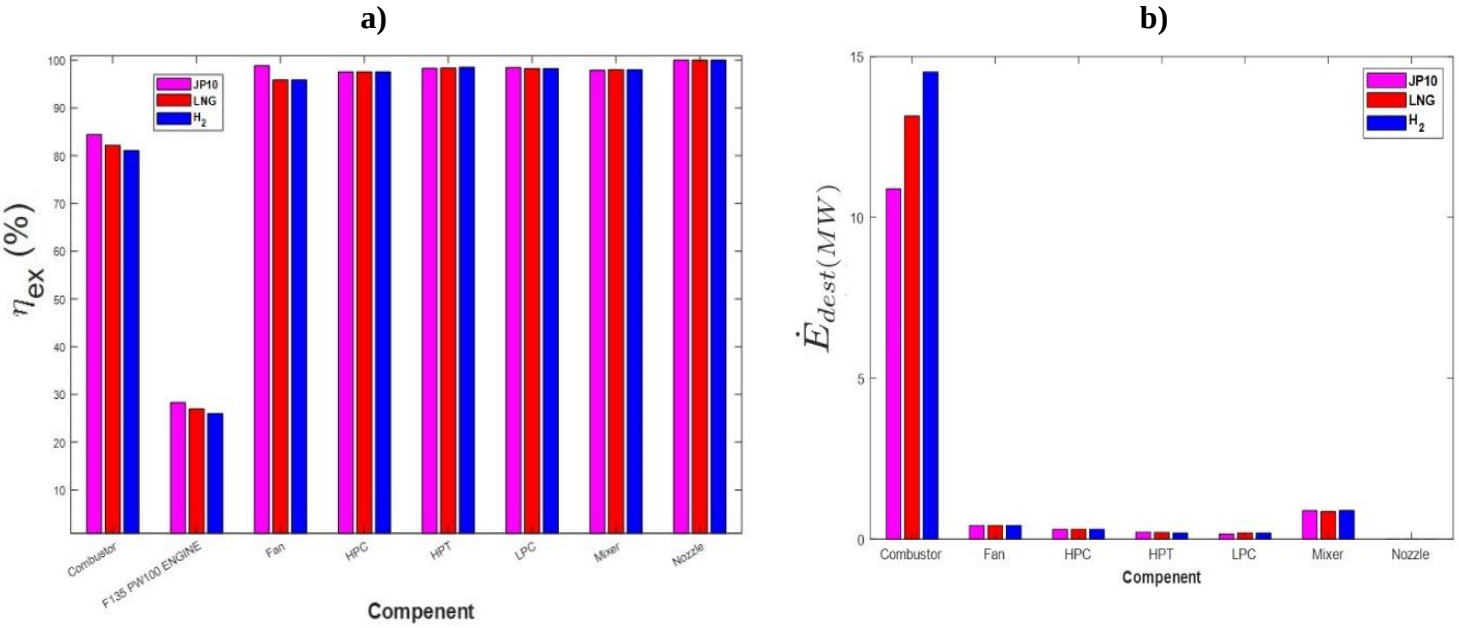

Fig. 10. The efficacy fuel types of the F135 PW100 engine and its components at a flight altitude of 20000 m and flight-Mach number of 2 on a) exergetic efficiency, and b) exergy destruction.

5.3. Deep learning results

Based on the results obtained in subsections 5.1 and 5.2, to model the thermodynamic performance of the F135 PW100 engine cycle, flight-Mach number and flight altitude are considered to be 2.5 and 30,000 m, respectively, due to the operational advantage of supersonic flying at high altitude, and higher thrust of hydrogen fuel. Accordingly, the appropriate datasets are provided and then randomly divided into two sets: the first set contains 6079 samples for model training and the second set contains 1520 samples for testing. Fig. 11 shows the relationship between all inputs and outputs. In the present deep neural network model, five input variables including the pressure ratio of the high-pressure compressor, fan pressure ratio, turbine inlet temperature, intake air temperature, and bypass ratio (α) are considered as the characteristics of the model and three output variables consist of thrust, thrust specific fuel consumption, the exergetic efficiency as labels. The data were extracted from python 3.9 software. To facilitate the training process, the input variables are normalized between zero and one. In this study, the Adam optimization algorithm, the cost function of the mean square error, and the active function of Relu are used to train the network. The final deep network prototypical, as shown in Fig. 10, has three hidden layers, the first to third layers have 512, 256, and 128 neurons, respectively, which are manually adjusted based on experience.

The loss function diagram in terms of each epoch is shown in Fig. 12 for each of the outputs such as thrust, TSFC, and exergetic efficiency. The results show a stable convergence process that has reached a very small amount for each output. The convergence trend is similar for all three outputs, although the final loss value of exergetic efficiency is greater than the TSFC, and the TSFC is greater than the thrust. This is due to the difference in the level of the output values that are observed in the plot (see the scales of outputs parameters such as thrust, TSFC, and exergetic efficiency) . It is also observed that for each of the outputs, on average in the first ten epochs, the loss function is reduced by 90%.

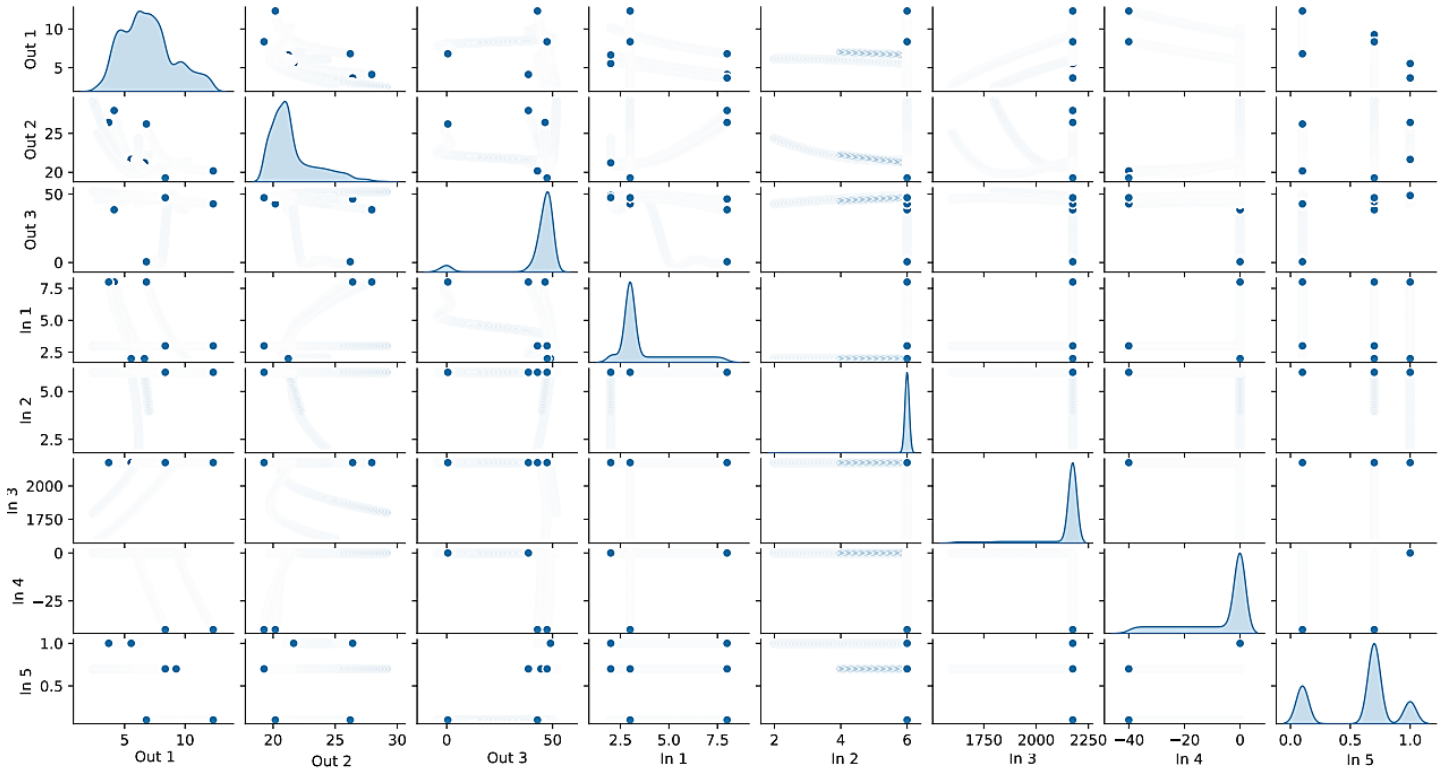

Fig. 11. The general plot of input and output variable relationships

To show the performance of the deep learning method in predicting outputs, Fig. 13 shows the predicted value of thrust, TSFC, and exergetic efficiency with respect to the True values in the test section. It can be seen that the deep neural model has been very successful in predicting outputs; Because the blue points inside the diagrams are very close to the midline $P = T$. This means that the predicted value is very close to the corresponding true value. In some of these diagrams, it can be seen that the data aggregation and also the distance of some of them from the centerline is greater, which indicates the greater numbers of data in these areas and, consequently, the greater the probability of error. For example, to predict the second output (TSFC), the accumulation of blue dots is greater in the range $21 \leq TSFC \leq 22$.

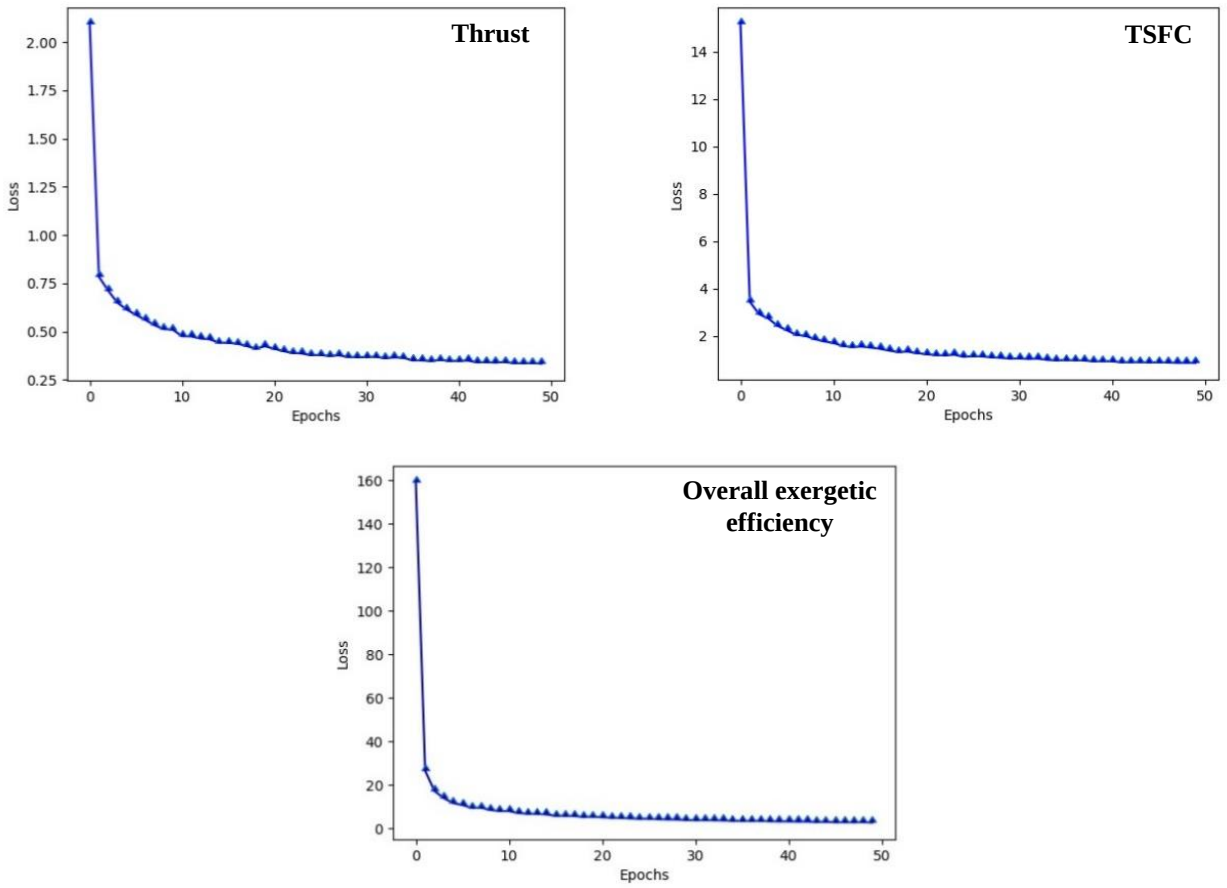

Fig. 12. Loss function variations with respect to Epochs for outputs variables.

Fig. 14 shows the error distribution of the 1520 test sample. For the thrust, 1347 samples (88.61%) are in the error range ± 1. Also, for the TSFC and exergetic efficiency, 1424 and 1381 samples, respectively, equivalent to 93.68% and 90.85% of the data are in the same error range. This high error distribution in the near-zero range indicates the success of the deep neural network in predicting test data.

Also, in order to measure the accuracy of the obtained model, the correlation factor (R), determination factor (R^2), root mean square error (RMSE), mean square error (MSE), mean absolute error (MAE), and mean absolute percentage error (MAPE) are utilized. The values of RMSE, MSE, and MAE express the difference between the predicted outputs and the true values. The closer these coefficients are to zero, the lower the error (higher accuracy) of the model.

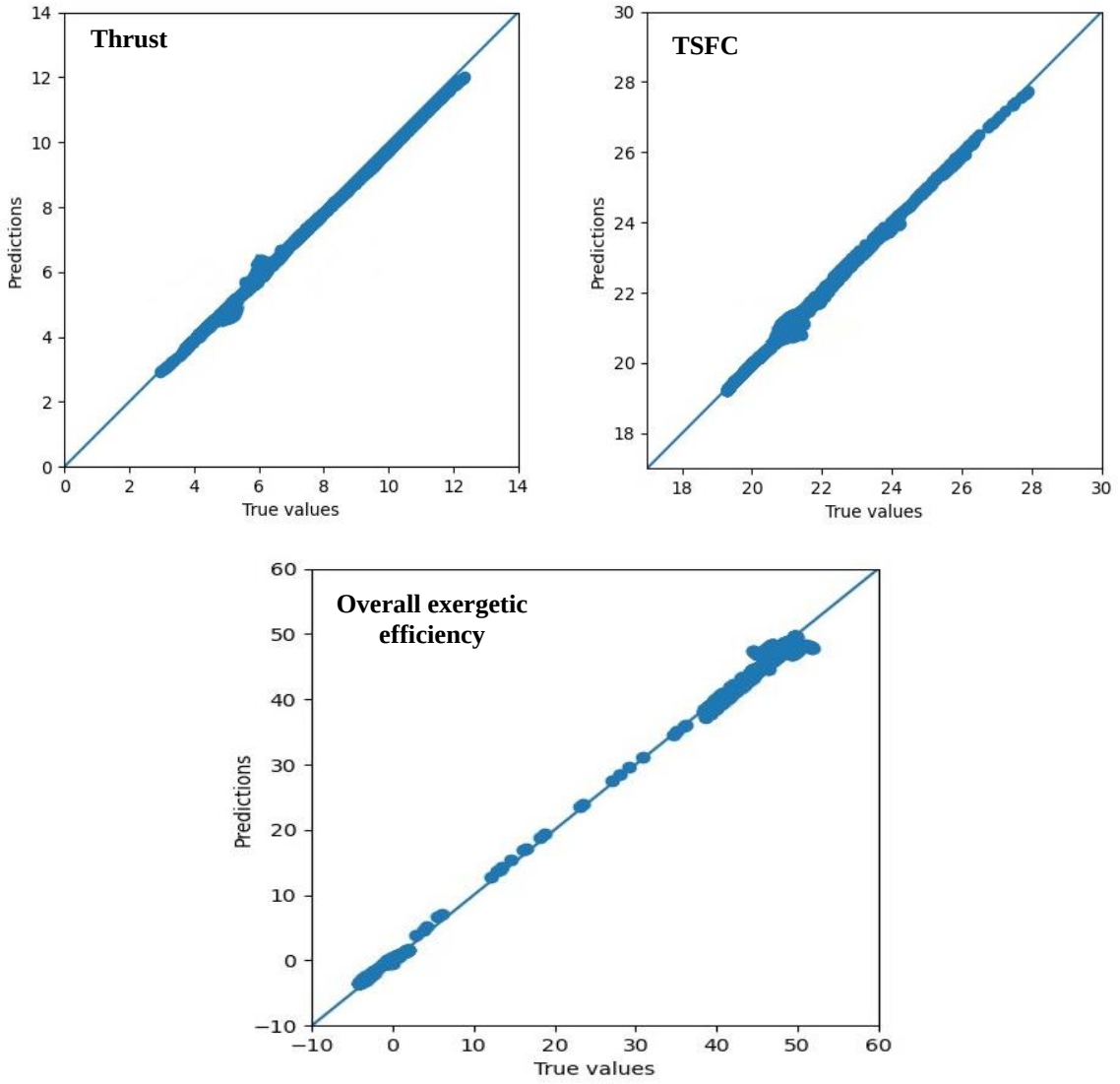

Fig. 13. Predicted output values with respect to true values.

The correlation and determination coefficients represent the correlation between the true values and the data predicted from the deep neural model. The closer the values of R and R^2 to one, the closer the estimated values are to the true values. Finally, the Mean absolute percentage error provides a good indication of the accuracy of the obtained model. In general, the RMS, MSE, and MAE criteria depend on the amplitude of the output values, while the R, R^2, and MAPE coefficients can ignore the amplitude effect and provide a relative comparison. All the desired indicators are defined as follows:

$$R = \frac{\sum_{i=1}^{n}[(y_i - y_i^{mean})(\hat{y}_i - \hat{y}_i^{mean})}{\sqrt{[\sum_{i=1}^{n}(y_i - y_i^{mean})^2][\sum_{i=1}^{n}(\hat{y}_i - \hat{y}_i^{mean})^2]}} \quad (58)$$

$$R^2 = \frac{[\sum_{i=1}^{n}(y_i - y_i^{mean})(\hat{y}_i - \hat{y}_i^{mean})]^2}{[\sum_{i=1}^{n}(y_i - y_i^{mean})][\sum_{i=1}^{n}(\hat{y}_i - \hat{y}_i^{mean})]} \quad (59)$$

$$RMSE = \frac{1}{n}\sum_{i=1}^{n}(y_i - \hat{y}_i)^2 \quad (60)$$

$$MAE = \frac{1}{n}\sum_{i=1}^{n}|y_i - \hat{y}_i| \quad (61)$$

$$MAPE = \frac{100\%}{n}\sum_{i=1}^{n}\left|\frac{y_i - \hat{y}_i}{y_i}\right| \quad (62)$$

where y_i is the true values for i-sample, $\hat{y}_i$ is the output predicted by the deep model for i- sample, y_i^{mean} is the mean of true values and $\hat{y}_i^{mean}$ is the mean of predicted data. The index is listed for two training and test sections as shown in Table 4. To predict the first output, it is observed that the indicators R and R^2 are 0.96 and 0.93, respectively. Also, the values of RMSE, MSE, and MAE are in the range of 0.5 and even lower. Also, the MAPE is about 5%; due to the mentioned values, the accuracy of the deep neural network is evaluated as very high. For the second output, R and R^2 are about 0.93 and 0.86, respectively. Error index values are also low and MAPE is about 1.5%. As a result, the success of the deep learning method in predicting the second output is also evident. Finally, for the third output, the R and R^2 indices are 0.99 and 0.99, respectively, which is very close to 1, indicating a very high correlation between the predicted and the true values. Also, the MAPE is calculated below 3%. As a result, it can be seen that the highest correlation coefficients belong to the third output, and the lowest MAPE value belongs to the second one. The first output also achieves a balance between the two indices. In general, the network accuracy of all outputs is evaluated as very high. It is noteworthy that with the aid of the attained intelligent model, the behavior of the considered engine can be analyzed and predicted in different flight conditions. It can also be determined whether the engine performance is optimal or whether it is necessary to

use the optimization algorithm to achieve better energy and exergy performances of a turbofan engine, in the future study.

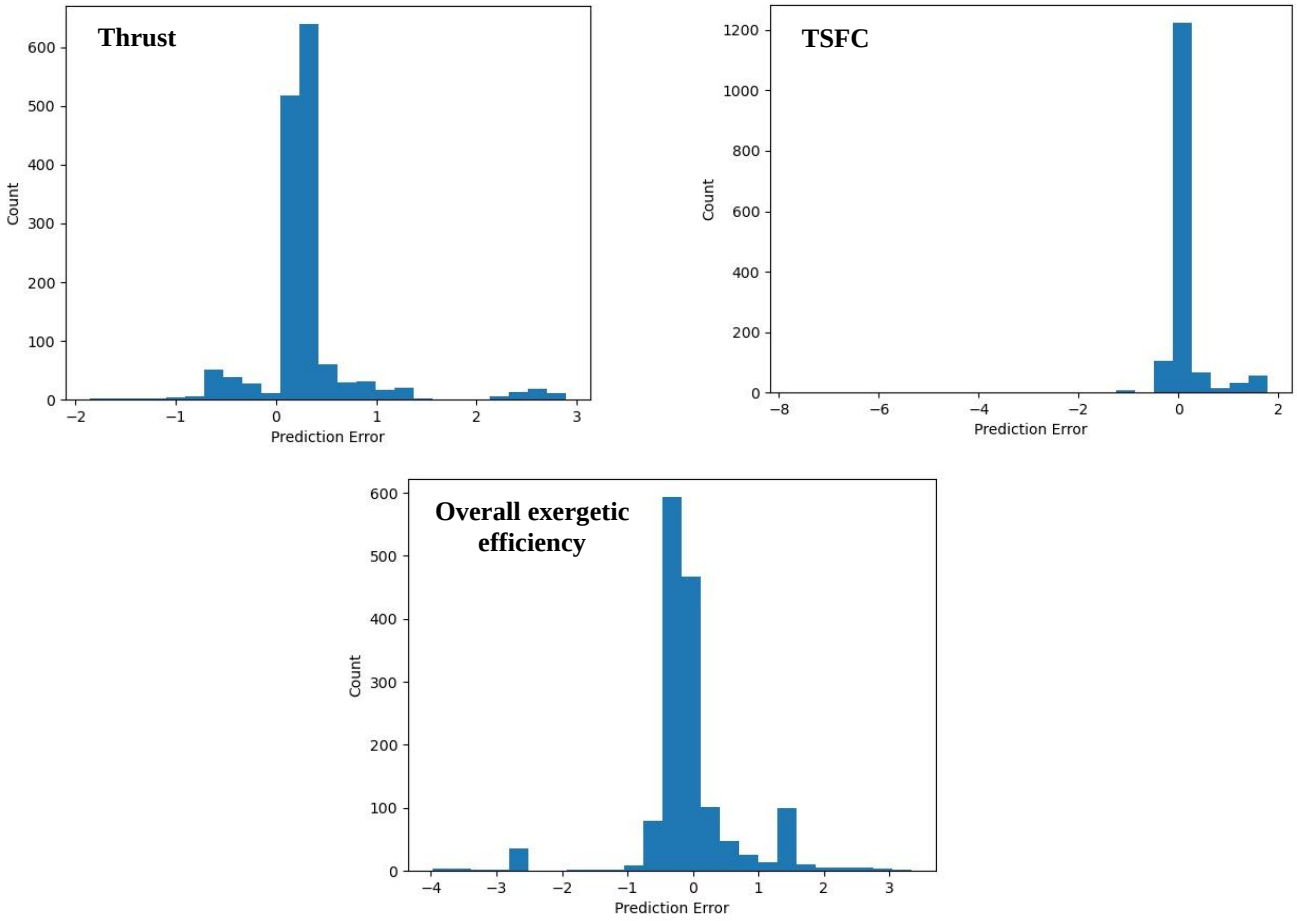

Fig. 14. Error distribution of the test samples for output variables.

Table 4. Indicator values in the learning and testing sections.

	Thrust		**TSFC**		**Overall exergetic efficiency**	
	Train	Test	Train	Test	Train	Test
R	0.9676	0.9686	0.9302	0.9276	0.9982	0.9982
R^2	0.9362	0.9383	0.8653	0.8604	0.9964	0.9965
RMSE	0.545	0.5367	0.7003	0.6966	0.8281	0.8118
MSE	0.297	0.288	0.4904	0.4853	0.6858	0.6591
MAE	0.3024	0.3013	0.3256	0.3164	0.5641	0.5604
MAPE	5.1216	5.023	1.4713	1.4393	2.1154	2.9212

6. Conclusion

In the present study, the thermodynamic analysis and intelligent modeling of the F135 PW100 engine have been performed. Particularly, a deep neural model was developed to predict the performance of the considered turbofan engine for flight-Mach number of 2.5 and the flight altitudes of 30,000 meters, which can be used to optimize the energy and exergy performances of a F135 PW100 engine. Based on the performed analyzes, the most important findings are as follows:

1) At constant flight altitudes, as the flight-Mach number increases, the intake mass flow rate to the engine rises, resulting in an increase in thrust, thrust specific fuel consumption, and propulsive efficiency. Also, in the same condition, the exergy efficiency of the low-pressure turbine decreases while that of the combustion chamber and mixer increases.
2) At constant flight-Mach number, as the flight altitude increases, the intake mass flow rate to the engine decreases, which in turn decreases the thrust and increases the thrust specific fuel consumption.
3) As the inlet air temperature in the engine decreases, the intake mass flow rate increases, resulting in an increase in thrust and thermal efficiency and the reduction of thrust-specific fuel consumption and propulsive efficiency. Also, in the same condition, the exergetic efficiency of high-pressure turbine, low-pressure turbine, and high-pressure compressor increases while that of the combustion chamber decreases.
4) It was found that among the considered fuels, hydrogen fuel has the highest thrust and thermal efficiency as well as the lowest propulsive efficiency. Conversely, using JP10 fuel results in lower thrust and thermal efficiency and higher propulsive efficiency.
5) The correlation factor for the prediction of thrust, thrust-specific fuel consumption, and overall exergetic efficiency is calculated as 0.96, 0.93, and 0.99, respectively. Moreover, the mean absolute percentage error for the aforementioned outputs are 5.02%, 1.43%, and 2.92%. Accordingly, the accuracy of a deep neural network for predicting all considered outputs is evaluated as very high.
6) According to the obtained deep neural model, the behavior of the considered engine in different flight conditions can be predicted and analyzed. For future study, the engine parameters can also be optimized to achieve better energy and exergy performances of a turbofan engine.

References

[1] A. El-Sayed, M. Emeara, M. El-habet. Performance Analysis of High Bypass Ratio Turbofan Aeroengine. International Journal of Development Research. 6 (2016) 8382-98.
[2] C.A. Saias, A. Pellegrini, S. Brown, V. Pachidis. Three-spool turbofan pass-off test data analysis using an optimization-based diagnostic technique. Proceedings of the Institution of Mechanical Engineers, Part A: Journal of Power and Energy. (2021) 09576509211002311.
[3] O. Balli, S. Ekici, T.H. Karakoc. TF33 Turbofan engine in every respect: Performance, environmental, and sustainability assessment. Environmental Progress & Sustainable Energy. 40 (2021) e13578.
[4] H. Chen, C. Cai, S. Jiang, H. Zhang. Numerical modeling on installed performance of turbofan engine with inlet ejector. Aerospace Science and Technology. 112 (2021) 106590.
[5] G. Xu, J. Sun, J. Wen, B. Dong, L. Zhuang, Q. Liu. Performance evaluation of a novel re-cooled mixed-flow turbofan cycle for aviation power application. Journal of Thermal Analysis and Calorimetry. 143 (2021) 3655-66.
[6] A.N. Rao, I. Goulos, D.G. MacManus. Impact of installation on a civil large turbofan exhaust system at idle descent conditions. Aerospace Science and Technology. 119 (2021) 107125.
[7] O. Balli, H. Caliskan. Turbofan engine performances from aviation, thermodynamic and environmental perspectives. Energy. 232 (2021) 121031.
[8] O. Balli, E. Ozbek, S. Ekici, A. Midilli, T. Hikmet Karakoc. Thermodynamic comparison of TF33 turbofan engine fueled by hydrogen in benchmark with kerosene. Fuel. 306 (2021) 121686.
[9] H.Y. Akdeniz, O. Balli. Impact of different fuel usages on thermodynamic performances of a high bypass turbofan engine used in commercial aircraft. Energy. 238 (2022) 121745.
[10] T.K. Ibrahim, F. Basrawi, O.I. Awad, A.N. Abdullah, G. Najafi, R. Mamat, et al. Thermal performance of gas turbine power plant based on exergy analysis. Applied Thermal Engineering. 115 (2017) 977-85.
[11] X. Zhao, O. Thulin, T. Grönstedt. First and Second Law Analysis of Intercooled Turbofan Engine. Journal of Engineering for Gas Turbines and Power. 138 (2015).
[12] H. Aygun, O. Turan. Exergetic sustainability off-design analysis of variable-cycle aero-engine in various bypass modes. Energy. 195 (2020) 117008.
[13] Y. S.H. Najjar, I. A.I. Balawneh. Optimization of gas turbines for sustainable turbojet propulsion. Propulsion and Power Research. 4 (2015) 114-21.
[14] E.S. Hendricks, J.S. Gray. pyCycle: A Tool for Efficient Optimization of Gas Turbine Engine Cycles. Aerospace. 6 (2019).
[15] R. Xue, J. Jiang, A. Jackson. Effect of Bypass Ratio on Optimal Fan Outer Pressure Ratio and Performance for Turbofan Engines. International Journal of Aeronautical and Space Sciences. 20 (2019) 157-64.
[16] O. Balli, Y. Sohret, H.T. Karakoc. The effects of hydrogen fuel usage on the exergetic performance of a turbojet engine. International Journal of Hydrogen Energy. 43 (2018) 10848-58.
[17] R.M.P. Gaspar, J.M.M. Sousa. Impact of alternative fuels on the operational and environmental performance of a small turbofan engine. Energy Conversion and Management. 130 (2016) 81-90.
[18] D. Verstraete. Long range transport aircraft using hydrogen fuel. International Journal of Hydrogen Energy. 38 (2013) 14824-31.

[19] P. Derakhshandeh, A. Ahmadi, R. Dashti. Simulation and technical-economic-environmental optimization of the General Electric GE90 hydrogen turbofan engine. International Journal of Hydrogen Energy. 46 (2021) 3303-18.
[20] G. Caposciutti, A. Baccioli, L. Ferrari, U. Desideri. Impact of ambient temperature on the effectiveness of inlet air cooling in a co-digestion biogas plant equipped with a mGT. Energy Conversion and Management. 216 (2020) 112874.
[21] K. Van Treuren, S. McClain. The Challenges of High Altitude Gas Turbine Engine Cycles2010.
[22] Z. Liu, I.A. Karimi. Gas turbine performance prediction via machine learning. Energy. 192 (2020) 116627.
[23] Q. Wang, L. Yang, K. Huang. Fast prediction and sensitivity analysis of gas turbine cooling performance using supervised learning approaches. Energy. 246 (2022) 123373.
[24] Y. Park, M. Choi, K. Kim, X. Li, C. Jung, S. Na, et al. Prediction of operating characteristics for industrial gas turbine combustor using an optimized artificial neural network. Energy. 213 (2020) 118769.
[25] A. Kaba, H. Aygun, O. Turan. Multi-dimensional energetic performance modeling of an aircraft engine with the aid of enhanced least–squares estimation based genetic algorithm method. Journal of Thermal Analysis and Calorimetry. (2021).
[26] D.J.R. Orozco, O.J. Venturini, J.C. Escobar Palacio, O.A. del Olmo. A new methodology of thermodynamic diagnosis, using the thermoeconomic method together with an artificial neural network (ANN): A case study of an externally fired gas turbine (EFGT). Energy. 123 (2017) 20-35.
[27] M.G. De Giorgi, M. Quarta. Hybrid MultiGene Genetic Programming - Artificial neural networks approach for dynamic performance prediction of an aeroengine. Aerospace Science and Technology. 103 (2020) 105902.
[28] T. Wang, D. Guo, X.-M. Sun. Remaining useful life predictions for turbofan engine degradation based on concurrent semi-supervised model. Neural Computing and Applications. (2021).
[29] D. Zhou, Q. Yao, H. Wu, S. Ma, H. Zhang. Fault diagnosis of gas turbine based on partly interpretable convolutional neural networks. Energy. 200 (2020) 117467.
[30] M. Talaat, M.H. Gobran, M. Wasfi. A hybrid model of an artificial neural network with thermodynamic model for system diagnosis of electrical power plant gas turbine. Engineering Applications of Artificial Intelligence. 68 (2018) 222-35.
[31] X. Zhou, J. Huang, F. Lu, J. Liu, C. Wang. HNN-based generalized predictive control for turbofan engine direct performance optimization. Aerospace Science and Technology. 112 (2021) 106602.
[32] Y. Tian, M.A. Chao, C. Kulkarni, K. Goebel, O. Fink. Real-time model calibration with deep reinforcement learning. Mechanical Systems and Signal Processing. 165 (2022) 108284.
[33] J.D. Mattingly, K.M. Boyer, H. von Ohain. Elements of propulsion: gas turbines and rockets. American Institute of Aeronautics and Astronautics Reston, VA2006.
[34] R.E. Sonntag, G.J. Van Wylen. Introduction to thermodynamics: classical and statistical. Wiley New York1991.
[35] O. Balli. Advanced exergy analysis of a turbofan engine (TFE): splitting exergy destruction into unavoidable/avoidable and endogenous/exogenous. International Journal of Turbo & Jet-Engines. 36 (2019) 305-27.

[36] M. Jagtenberg. Development Of A Preliminary Lifing Analysis Tool For The F135-PW-100 Engine. (2018).
[37] S. Kuczyński, M. Łaciak, A. Szurlej, T. Włodek. Impact of liquefied natural gas composition changes on methane number as a fuel quality requirement. Energies. 13 (2020) 5060.
[38] R. Su, Z. Yu, L. Xia, J. Sun. Performance analysis and multi-objective optimization of an integrated gas turbine/supercritical CO2 recompression/transcritial CO2 cogeneration system using liquefied natural gas cold energy. Energy Conversion and Management. 220 (2020) 113136.
[39] H. Lander, A. Nixon. Endothermic fuels for hypersonic vehicles. Journal of Aircraft. 8 (1971) 200-7.
[40] L. Maurice, T. Edwards, J. Griffiths. Liquid hydrocarbon fuels for hypersonic propulsion. Scramjet propulsion, Reston, VA, American Institute of Aeronautics and Astronautics, Inc, 2000. (2000) 757-822.
[41] E. Goodger. Hydrocarbon Fuels: Production. Properties and Performance of Liquids and Gases. (1975).
[42] S. Li, B. Varatharajan, F. Williams. Chemistry of JP-10 ignition. AIAA journal. 39 (2001) 2351-6.
[43] L. Türker, S. Variş, Ç.Ç. Bayar. A theoretical study of JP-10 hydroperoxidation. Fuel. 104 (2013) 128-32.
[44] National Center for Biotechnology Information (2021). PubChem Compound Summary for CID 11159354, Exo-Trimethylenenorbornane. Retrieved December 31, 2021 from https://pubchem.ncbi.nlm.nih.gov/compound/Exo-Trimethylenenorbornane.
[45] R. Papagiannakis. Comparative Evaluation of the effect of partial substitution of diesel fuel by natural gas on performance and emissions of a fumigated dual fuel diesel engine. International Journal of Energy and Environmental Engineering. 2 (2011) 31-43.
[46] P. Sforza. Propulsion principles and engine classification. Theory of Aerospace Propulsion e A Volume in Aerospace Engineering, second ed Butterworth-Heinemann, Elsevier, Oxford United Kingdom, pp 1e52. (2017).
[47] P. Gunasekar, S. Manigandan, V. S, R. Gokulnath, R. Vimal, P. Boomadevi. Effect of hydrogen addition on exergetic performance of gas turbine engine. Aircraft Engineering and Aerospace Technology. 92 (2020) 180-5.
[48] Y.-G. Li. Aero gas turbine flight performance estimation using engine gas path measurements. Journal of Propulsion and Power. 31 (2015) 851-60.
[49] H. Aygun, O. Turan. Application of genetic algorithm in exergy and sustainability: A case of aero-gas turbine engine at cruise phase. Energy. 238 (2022) 121644.
[50] E.O. Osigwe, A. Gad-Briggs, T. Nikolaidis, S. Jafari, B. Sethi, P. Pilidis. Thermodynamic Performance and Creep Life Assessment Comparing Hydrogen-and Jet-Fueled Turbofan Aero Engine. Applied Sciences. 11 (2021) 3873.
[51] M.R. Majdi Yazdi, F. Ommi, M.A. Ehyaei, M.A. Rosen. Comparison of gas turbine inlet air cooling systems for several climates in Iran using energy, exergy, economic, and environmental (4E) analyses. Energy Conversion and Management. 216 (2020) 112944.